

Transport properties of a periodically driven superconducting single electron transistor

Alessandro Romito

*Department of Condensed Matter Physics, The Weizmann Institute of Science, Rehovot 76100, Israel and
NEST-CNR-INFM & Scuola Normale Superiore, Piazza dei Cavalieri 7, I-56126 Pisa, Italy*

Simone Montangero

NEST-CNR-INFM & Scuola Normale Superiore, Piazza dei Cavalieri 7, I-56126 Pisa, Italy

Rosario Fazio

*International School for Advanced Studies (SISSA) via Beirut 2-4, I-34014, Trieste, Italy and
NEST-CNR-INFM & Scuola Normale Superiore, Piazza dei Cavalieri 7, I-56126 Pisa, Italy*

(Dated: February 8, 2020)

We discuss coherent transport of Cooper pairs through a Cooper pair shuttle. We analyze both the DC and AC Josephson effect in the two limiting cases where the charging energy E_C is either much larger or much smaller than the Josephson coupling E_J . In the limit $E_J \ll E_C$ we present the detailed behavior of the critical current as a function of the damping rates and the dynamical phases. The AC effect in this regime is very sensitive to all dynamical scales present in the problem. The effect of fluctuations of the external periodic driving is discussed as well. In the opposite regime the system can be mapped onto the quantum kicked rotator, a classically chaotic system. We investigate the transport properties also in this regime showing that the underlying classical chaotic dynamics emerges as an incoherent transfer of Cooper pairs through the shuttle. For an appropriate choice of the parameters the Cooper pair shuttle can exhibit the phenomenon of dynamical localization. We discuss in details the properties of the localized regime as a function of the phase difference between the superconducting electrodes and the decoherence due to gate voltage fluctuations. Finally we point how dynamical localization is reflected in the noise properties of the shuttle.

PACS numbers:

I. INTRODUCTION

Soon after the appearance of the microscopic theory of superconductivity¹, Josephson predicted a remarkable manifestation of macroscopic quantum coherence² by showing that two superconducting electrodes connected by an insulating barrier can sustain a dissipationless current. Since its discovery, the Josephson effect has had a tremendous impact both in pure^{3,4} and applied physics⁴. One of the most recent and exciting developments in the research based on the Josephson effect is probably in the implementation of superconducting nanocircuits for solid state quantum computation⁵.

In nanodevices a new energy scale appears, the charging energy, and new interesting effects show up due to the interplay between Josephson coupling and the presence of charging. The Josephson coupling, leading to phase coherence between the two superconducting electrodes can be understood in terms of the coherent superposition of different charge states. Coulomb blockade⁶ on the other side tends to localize the charge thus destroying phase coherence. The simplest example of this interplay is provided by behavior of the supercurrent through a Superconducting Single Electron Transistor (SSET)³. It consists in a small superconducting island connected, by tunnel junctions, to two superconducting electrodes.

Additional features emerge if the SSET is coupled to mechanical degrees of freedom thus combining the field

of single electron effects with the intensively studied area of Nano-ElectroMechanical systems⁷. Among the most interesting devices in this area there is the electron shuttle (for a review see Ref. 8). In its essential realization, a shuttle system consists of a small conducting grain, in Coulomb blockade regime, oscillating periodically between two electrodes (source and drain). The essential condition to characterize the shuttling mechanism is that the grain must be in contact with a single electrode at any time. Following the original proposal of a normal shuttle Gorelik *et al.*⁹ introduce the *Cooper pair shuttle* where all the device (electrodes and central island) is in the superconducting state. Despite the fact that the central island is never connected to the two superconductors simultaneously, the Chalmers group has shown that the system is still capable to establish a global phase coherence and hence support a finite Josephson current^{9,10}. The shuttle does not only carry charge, as in the normal metal case, but it also establishes phase coherence between the superconductors. Differently from the normal case, the Cooper pair shuttle does not need a moving island, it is just a SSET with time dependent Josephson couplings and therefore it can be realized in the standard SSET with time-dependent fluxes¹¹. The properties of the Cooper pair shuttle crucially depend on the decoherence mechanism which is also responsible in driving the system toward a steady state. The presence of dissipation modifies the current phase relation, but does not (in general) destroy the Josephson current^{9,11}. The

effect of gate voltage fluctuations has been analyzed in Ref. 11 where it has been shown that decoherence can even enhance the Josephson current. Additional work on the Cooper pair shuttle considered the full counting statistics of Cooper pair shuttling¹², and the possibility of observing quantum chaotic dynamics¹³.

The present paper extends our previous works on the subject^{11,13}. In the limit $E_J/E_C \ll 1$ we provide details of the derivation of DC Josephson current and consider several extensions which are important for a connection with possible experiments. We analyze the effect of fluctuations in the external driving and the effect of an external voltage. In addition we discuss the AC effect and study the interplay of various times cales on the spectrum of the AC current. In the opposite limit $E_J/E_C \gg 1$ we present analytical and numerical results on the dynamical localization and discuss its signatures on the Josephson current fluctuations.

The paper is organized as follows. In Section II we present the model of the Cooper pair shuttle. In Section III we analyze the transport properties of the shuttle in the Coulomb blockade regime. We present the details of the formalism to determine the steady state density matrix, and to derive the steady state Josephson current, whose physical features are discussed in Subsection III C. Subsections III D and III E are dedicated respectively to the effect of fluctuations of the external driving on the Josephson current and to the effect of an applied voltage bias, the AC Josephson effect. The chaotic regime of the Cooper pair shuttle is the subject of Section IV. We discuss the dynamics of the charge in the central island, in Subsection IV A. A new feature which appear as compared to the kicked rotator is an extra phase shift during the kicks which is due to the superconducting phase difference of the electrodes. This phase shift plays a key role since it is responsible for time reversal symmetry breaking whose consequences for the dynamics are investigated in Subsection IV B. In Sections IV C we develop the necessary formalism to calculate the full counting statistics in the chaotic regime. The concluding remarks are presented in Section V. Several technical details are given in the Appendices A, B and C. Throughout the paper $k_B = 1$.

II. THE MODEL

The Cooper pair shuttle is schematically shown in Fig. 1. It consists of a central island connected to two superconducting electrodes and capacitively coupled to a gate voltage. The superconducting island is small enough such that charging effects have to be included. The two leads are macroscopic and their phases $\phi_{L,R}$ can be treated as classical variables. The couplings of the island to the leads are time-dependent. This time dependence is given by external means and can be achieved either by making the island to move or by tuning in time magnetic fluxes and gates. This has to be contrasted with the case

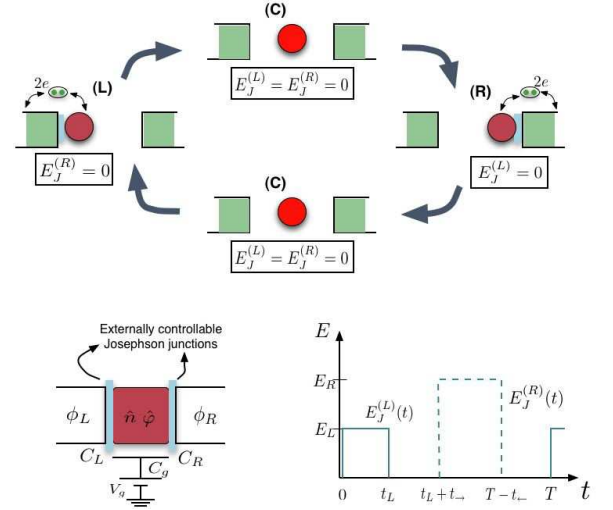


Figure 1: Upper left panel. Schematic representation of the system described by the Hamiltonian Eq. (1). It consists of a Cooper pair box coupled through externally switched Josephson junctions to phase biased superconductors. Upper right panel. Time dependence of the left and right Josephson energies within a single period. Lower panel. Sketch of the Cooper pair shuttle's cycle. The three intervals L, C and R, within the period $T = t_L + t_{\rightarrow} + t_R + t_{\leftarrow}$, correspond to the situations: (L) $E_J^{(L)}(t) = E_L$, $E_J^{(R)}(t) = 0$ (interaction time at left lead); (C) $E_J^{(L)}(t) = 0$, $E_J^{(R)}(t) = 0$ (free evolution time in forward and backward directions); (R) $E_J^{(L)}(t) = 0$, $E_J^{(R)}(t) = E_R$ (interaction time at right lead).

of single electron shuttle where for the implementation of the shuttle a mechanical moving island is necessary^{14,15}.

The system is described by the following Hamiltonian

$$H_0 = E_C(t)[\hat{n} - n_g(t)]^2 - \sum_{b=L,R} E_J^{(b)}(t) \cos(\hat{\varphi} - \phi_b). \quad (1)$$

In Eq.(1) \hat{n} is the number of excess Cooper pairs in the central island and $\hat{\varphi}$ is its conjugate phase, $[\hat{n}, \hat{\varphi}] = -i$. The charging energy is given by $E_C(t) = (2e)^2/2C_\Sigma(t)$ with $C_\Sigma(t) = C_g(t) + C_L(t) + C_R(t)$ the total capacitance of the SSET ($C_{L/R/g}$ are the various capacitances indicated in Fig. 1), $E_J^{(L,R)}(t)$ are the Josephson couplings to the left or right lead respectively, and $n_g(t) = C_g(t)V_g(t)/2e$ is the gate charge which can be tuned via the gate voltage V_g .

The Hamiltonian in Eq. (1) is nothing else than a SSET with an external drive contained in the time dependence (described in Fig. 1) of the Josephson energies and of the gate voltage. The island is said to be in contact with one of the leads when the corresponding Josephson coupling is non-zero (with value E_L , E_R) (configurations L and R in Fig.1). In the intermediate region (configuration C), $E_J^{(L)}(t) = E_J^{(R)}(t) = 0$. Note that both Josephson coupling are never on at the same time. As in Ref. 10 we employ a sudden approximation (which requires a switching

time $\Delta t \ll \hbar/E_{L(R)}$ and suppose $E_J^{(L,R)}(t)$ to be step functions in each region (see Fig. 1). For later convenience we define the functions

$$\Theta_L(t) = \theta(t)\theta(t_L - t), \quad (2)$$

$$\Theta_R(t) = \theta(t - (t_L + t_{\rightarrow}))\theta(t_L + t_{\rightarrow} + t_R - t), \quad (3)$$

in order to write the time dependent Josephson energies as

$$E_J^{(b)}(t) = E_b \sum_{n \in \mathbb{N}} \Theta_b(t - nT), \quad b \in \{L, R\} \quad (4)$$

The total capacitance $C_{\Sigma}(t)$ is weakly dependent on time at the contact regions⁴⁷ and therefore we assume it to be constant during the intervals L and R (obviously the same hold for $E_C(t) = E_C$). In the intermediate region (C) it is not necessary to specify the exact time dependence of $E_C(t)$, as it will be clear in Section III.

In the rest of the paper we study the transport properties of the Cooper pair shuttle. The transfer of charge is expressed by the presence of a current at left and right contacts. The corresponding current operators are, in the Schrödinger picture,

$$\hat{I}_L(t) = 2e \frac{E_L}{\hbar} \sin(\hat{\varphi} - \varphi_L) \Theta_L(t), \quad (5)$$

$$\hat{I}_R(t) = 2e \frac{E_R}{\hbar} \sin(\hat{\varphi} - \varphi_R) \Theta_R(t), \quad (6)$$

corresponding to the coherent exchange of Cooper pairs between the grain and the left or right lead respectively. Due to the periodical external driving, any interaction with the external environment leads to a steady state, where every observable is periodic. We will essentially ignore transient effects and concentrate on the stationary values of physical observables.

A. Cooper pair shuttle with time-dependent fluxes

Before analyzing in detail the transport properties, we discuss a way to realize a Cooper pair shuttle which does not require any mechanically moving part. Here the time dependence of the Josephson couplings and n_g is obtained by a time dependent magnetic field and gate voltage, respectively. The setup consists of a more complicated superconducting nanocircuit in a uniform magnetic field as sketched in Fig.2. By substituting each Josephson junction by SQUIDS, it is possible to control the $E_J^{(b)}(t)$ by tuning the applied magnetic field piercing the loop. The presence of three type of loops with different area, A_L, A_R, A_C allows to achieve independently the three cases, where one of the two E_J 's is zero (regions L,R) or both of them are zero (region C), by means of a *uniform* magnetic field. If the applied field is such that a half-flux quantum pierces the areas A_L, A_R or A_C , the Josephson couplings will be those of regions R,L and C, respectively and the Hamiltonian of the system can be exactly mapped onto that of Eq.(1). Moreover, by choosing

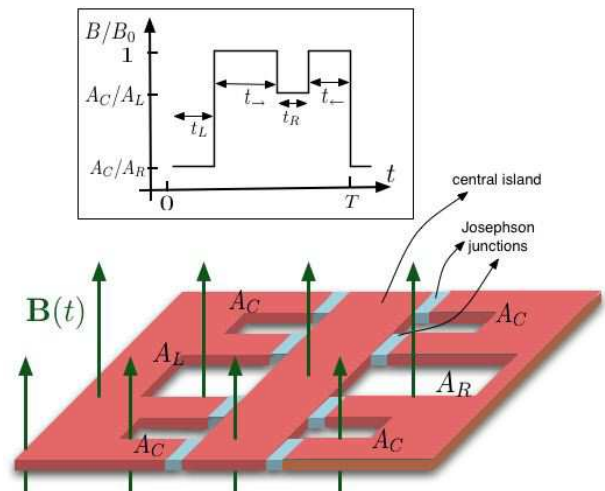


Figure 2: The setup for the implementation of the shuttle process by means of a time-dependent magnetic field. The inset shows the time dependence of the applied field (in unity of $B_0 = \Phi_0/(2A_C)$, Φ_0 is the flux quantum) in order to realize Cooper pair shuttling. The different loop areas can be chosen in order to obtain $E_L = E_R$.

the ratios $A_C/A_R = 0.146$, and $A_C/A_L = 0.292$ the two Josephson coupling are equal, $E_L = E_R = E_J$. This implementation has several advantages. It allows to control the coupling with the environment by simply varying the time dependence of the applied magnetic field. The time scale for the variation of the magnetic field should be controlled at the same level as it is done in the implementation of Josephson nanocircuits for quantum computation (see Ref. 5 for an extensive discussion).

For a quantitative comparison with the results described here, the magnetic field should vary on a time scale shorter than \hbar/E_J , typically a few nanoseconds with the parameters of Ref. 16. This is possible with present day technology¹⁷. At a qualitative level the features of the Josephson current presented in this paper do not rely on the step-change approximation of the Josephson couplings. These effects are observable even if the magnetic field changes on time-scales comparable or slower than E_J . The only strict requirement is that only one Josephson coupling at the time is switched on.

III. COULOMB BLOCKADE REGIME

We first consider the system when $E_L, E_R \ll E_C$, *i.e.* in the Coulomb blockade regime. In addition, the gate voltage is chosen so that $0 < n_g(t) \leq 1/2$. Namely $n_g(t) = 1/2$ when the system is in contact with one of the lead and $n_g(t) = \text{const.} \in (0, 1/2)$ in the remaining time of the cycle. Our choice (the same of Ref. 9) results in having exact charge degeneracy during the Josephson contacts, then enhancing charge transfer. A different condition, of easier experimental realization, in which

$n_g(t) = \text{const.}$ is discussed in Appendix A. In this limit one can restrict the Hilbert space of the system to the one spanned by the two charge states $\{|n=0\rangle, |n=1\rangle\}$. The Hamiltonian of the system restricted to the two dimensional vector space, reads

$$\hat{H}_0 = E_C(t) \left[\frac{1}{2} - n_g(t) \right] \sigma_z - \sum_{b=L,R} \frac{E_J^{(b)}(t)}{2} (e^{-i\phi_b} \sigma_+ + \text{h.c.}) \quad (7)$$

where we used the 2×2 Pauli matrices σ_i ($i = x, y, z$) with the standard notation $\sigma_{\pm} = (\sigma_x \pm \sigma_y)/2$.

In order to evaluate the current, Eqs.(5,6), or the average value of any observable, we need to compute the reduced density matrix of the central island $\rho(t)$. The steady state density matrix depends on the specific decoherence mechanism. The main source of decoherence in the Cooper pair shuttle is due to gate voltage fluctuations, either induced by the electromagnetic environment or by background charges.

A. Classical noise

At a classical level voltage fluctuations can be included by adding a classical stochastic term to $n_g(t)$. The Hamiltonian in Eq. (7) is modified by the presence of the extra term,

$$\hat{H} = \hat{H}_0 + \xi(t) \sigma_z, \quad (8)$$

where $\xi(t)$ has a white noise spectrum

$$\begin{aligned} \langle \xi(t) \rangle_{\text{stoc}} &= 0 \\ \langle \xi(t) \xi(t') \rangle_{\text{stoc}} &= \hbar^2 \gamma \delta(t - t') \end{aligned}$$

where γ is the inverse decoherence time. If we neglected the fluctuations, the time evolution of the system would be fully coherent. By including fluctuations, the shuttle will be described by 2×2 density matrix that obeys the following Bloch equation:

$$\frac{\partial \hat{\rho}}{\partial t} = -\frac{i}{\hbar} \left(\hat{H}_0(t) \hat{\rho} - \hat{\rho} \hat{H}_0(t) \right) - 2\gamma (\hat{\rho} - \sigma_z \hat{\rho} \sigma_z). \quad (9)$$

The only stationary solution of this equation is trivial: $\hat{\rho} = \hat{1}/2$, this corresponds to the absence of any average superconducting current. This is a combined effect of the decoherence term and Josephson coupling. In the absence of Josephson coupling, voltage fluctuations can not cause transitions between the charge states so no relaxation takes place. With Josephson coupling switched on, the voltage fluctuations cause transitions between the stationary states separated by energy $E_J^{(L,R)}$. Classical voltage fluctuations result in equal transition rates with increasing and decreasing energy. The vanishing of the critical current has a simple explanation, the classical noise mimics a bath at infinite temperature. No coherence can be established at temperatures much higher than the Josephson coupling energy. Nevertheless this

model is worth to be considered because, as shown in Ref. 12 there is an high temperature regime where the average current is zero but still coherence manifests in the higher moments of current fluctuations. At low temperatures, $T_b \lesssim E_J^{(L,R)}$ the interactions with the bath can lead to a density matrix $\hat{\rho} \neq \hat{1}$ and then to a non-vanishing supercurrent.

B. Quantum noise

In order to analyze the low temperature regime, we need to take into account the quantum features of the bath. As the most important source of fluctuations in the charge regime are gate voltage fluctuation we couple the shuttle via the charge operator \hat{n} to an environment described by the Caldeira–Leggett model¹⁸,

$$H_{\text{int}} = \hat{n} \hat{\mathcal{O}} + H_{\text{bath}} = \hat{n} \sum_i \lambda_i (a_i + a_i^\dagger) + H_{\text{bath}}. \quad (10)$$

In Eq.(10), H_{bath} is the bath Hamiltonian, with boson annihilation/creation operators of the i -th mode a_i, a_i^\dagger , $H_{\text{bath}} = \sum_i \omega_i (a_i^\dagger a_i + 1/2)$. Due to the periodicity of the external driving the time evolution of the system at long time, $t \gg T$, can be determined by iterating the evolution of the density matrix $\rho(t)$ over one single period. This evolution can be computed through a linear map $\mathcal{M}_{t \rightarrow t+T}$ defined by

$$\rho(t+T) = \mathcal{M}_{t \rightarrow t+T} [\rho(t)]. \quad (11)$$

With the following choice of parametrizing $\rho(t) = 1/2 [\mathbb{1} + \sigma \cdot \mathbf{r}(t)]$, where $i = x, y, z$ and $r_i(t) = \langle \sigma_i \rangle$, the map in Eq. (11) assumes the form of a general affine map for the vector $\mathbf{r}(t)$:

$$\mathbf{r}(t+T) = M_t \mathbf{r}(t) + \mathbf{v}_t, \quad \mathbf{r} \in \mathcal{B}_1(\mathbf{0}) \subset \mathbb{R}^3 \quad (12)$$

where \mathcal{B}_1 is the Ball of unitary radius in \mathbb{R}^3 . The matrix M_t fulfills the property

$$|M_t \mathbf{v}| \leq |\mathbf{v}| \quad \forall \mathbf{v} \in \mathcal{B}_1(\mathbf{0}), \quad (13)$$

as we will see from its explicit form determined below.

In the long time limit, the system reaches a periodic steady state,

$$\mathbf{r}_\infty(t) = (\mathbb{1} - M_t) \mathbf{v}_t, \quad (14)$$

if, and only if, $\det(\mathbb{1} - M_t) \neq 0$. When this condition is not satisfied the external bath introduced in Eq. (10) is not effective and the system never loses memory of the initial conditions.

The stationary limit is the fixed point of $\mathcal{M}_{t \rightarrow t+T}$ ¹⁹. The expression of $\mathbf{r}_\infty(t)$, and therefore of $\rho_\infty(t) = 1/2 [\mathbb{1} + \sigma \cdot \mathbf{r}_\infty(t)]$, uniquely determines the steady state of the system.

The periodic time dependence of any physical observable A is given by

$$\langle \hat{A}(t) \rangle = \text{Tr} \{ \rho_\infty(t) \hat{A} \}, \quad (15)$$

where the operator \hat{A} is in the Shrödinger representation.

The assumption of a stepwise varying Hamiltonian considerably simplifies the form of the map $\mathcal{M}_{t \rightarrow t+T}$, which now can be expressed as a composition of the time evolutions of ρ in the intervals L, C, R (see Fig.1). In each time interval it is straightforward to solve the corresponding master equation for the reduced density matrix²⁰. In the portion of the cycle corresponding to the island being in contact with the left electrode the master equation reads

$$\dot{\mathbf{r}}(t) = G_L(t) \mathbf{r}(t) + 2\gamma_L \mathbf{w}_L \quad (16)$$

with $\mathbf{w}_L^\dagger = \tanh(E_L/T_b) (\cos \phi_L, \sin \phi_L, 0)$ and

$$G_L = \begin{pmatrix} -2\gamma_L & 0 & -\frac{E_L}{\hbar} \sin \phi_L \\ 0 & -2\gamma_L & -\frac{E_L}{\hbar} \cos \phi_L \\ \frac{E_L}{\hbar} \sin \phi_L & \frac{E_L}{\hbar} \cos \phi_L & 0 \end{pmatrix}. \quad (17)$$

Here, γ_L is the dephasing rate (for this portion of the cycle), depending on the temperature of the bath, which is taken in thermal equilibrium at temperature T_b . The master equation when the island is in contact with the right superconducting lead goes along the same lines with the substitution $L \rightarrow R$ (thus introducing a dephasing rate γ_R). Both dephasing rate can be obtained in the Born-Markov approximation²⁰, which requires that the bath autocorrelation time is the smallest time scale in the problem. This treatment is valid provided that $\gamma_{L(R)} \ll T_b/\hbar, E_{L(R)}/\hbar$, and that the time interval $t_{L(R)}$ is much longer than both $\hbar T_b^{-1}$ and $\hbar E_{L(R)}^{-1}$. As an example, for an Ohmic bath with coupling to the environment $\alpha \ll 1$, one has $\gamma_{L(R)} = (\pi/2)\alpha E_{L(R)} \coth(E_{L(R)}/2T_b)/\hbar$ ¹⁸. G_L is time independent as a consequence of the Born-Markov approximation. The solution of the master equation in the contact region can be obtained in the form

$$\mathbf{r}(t_L) = \exp(G_L t_L) \mathbf{r}(0) - 2\gamma_L G_L^{-1} \cdot [\mathbf{1} - \exp(G_L t_L)] \mathbf{w}_L. \quad (18)$$

The parameters of the Hamiltonian enter the final results only through the combinations $\theta_{L(R)} = E_{L(R)} t_{L(R)}/\hbar$ and $\gamma_{L(R)} t_{L(R)}$. Due to the condition $\gamma_{L(R)} \ll E_{L(R)}/\hbar$ the parameter $\hbar \gamma_{L(R)}/E_{L(R)}$ does not enter the results at lowest order.

During that part of the cycle when the island is disconnected from both electrodes, the situation is simpler. Since \hat{n} is conserved, the evolution can be determined exactly

$$\mathbf{r}(t_{\rightarrow} + t_L) = \exp(G_{\rightarrow} t_{\rightarrow}) \cdot R(\chi_{\rightarrow}) \mathbf{r}(t_L). \quad (19)$$

In the previous equation we defined

$$G_{\rightarrow} = \begin{pmatrix} -\gamma_{\rightarrow} & 0 & 0 \\ 0 & -\gamma_{\rightarrow} & 0 \\ 0 & 0 & 1 \end{pmatrix} \quad (20)$$

and

$$R(\chi_{\rightarrow}) = \begin{pmatrix} \cos(\chi_{\rightarrow}) & -\sin(\chi_{\rightarrow}) & 0 \\ \sin(\chi_{\rightarrow}) & \cos(\chi_{\rightarrow}) & 0 \\ 0 & 0 & 1 \end{pmatrix}. \quad (21)$$

where $\chi_{\rightarrow} = \int_{t_L}^{t_L+t_{\rightarrow}} E_C(t)(1 - 2n_g)/\hbar$. The rate γ_{\rightarrow} depends only on the properties of the bath. Its explicit time-dependence varies when the time scale is compared with the inverse ultraviolet bath mode cut-off, $1/\omega_c$, and the inverse bath temperature, \hbar/T_b ^{21,22}. An expression of γ_{\rightarrow} in terms of bath parameters can be obtained within the same Born-Markov approximation discussed above in the case of a weakly coupling between the bath and the system. It gives $\gamma_{\rightarrow} = 2\pi\alpha T_b/\hbar$ in which case γ_{\rightarrow} is independent on time and the decay is purely exponential. The same equation holds in the backward free evolution time

$$\mathbf{r}(T) = \exp(G_{\leftarrow} t_{\leftarrow}) \cdot R(\chi_{\leftarrow}) \mathbf{r}(T - t_{\leftarrow}), \quad (22)$$

where G_{\leftarrow} is defined as G_{\rightarrow} in Eq. (19) with the replacement $\gamma_{\rightarrow} \rightarrow \gamma_{\leftarrow}$. In addition to the dynamical phases $\chi_{\rightarrow(\leftarrow)}$ and $\theta_{L(R)}$, also the phase difference $\phi = \phi_L - \phi_R$ enters in determining the physical observables. The effect of damping is characterized by the dimensionless quantities $\gamma_{L(R)} t_{L(R)}$, and $\gamma_{\rightarrow(\leftarrow)} t_{\rightarrow(\leftarrow)}$.

From Eqs. (16-19) it is easy to check that M_t fulfills the property in Eq. 13 except for the following values $(\gamma_L, \gamma_R, \gamma_{\rightarrow}, \gamma_{\leftarrow}) = (0, 0, 0, 0)$ or $(\gamma_L, \gamma_R, \theta_L, \theta_R) = (0, 0, k\pi/2, h\pi/2)$, k, h integers, when $\det(\mathbf{1} - M_t) = 0$. In these cases, the system keeps memory of its initial conditions and it never approaches the steady state. This is however an artificial situation, because other sources of dissipation are present and will drive the system to a steady state.

C. DC Josephson current

The asymmetry between emission and absorption of quanta from the bath leads to a nontrivial fixed point (Eq. (14)) for the map \mathcal{M} , thus leading to a non vanishing Josephson current through the Cooper pair shuttle. The current depends on the quantum dynamical evolution of the charge on the island and on the interplay between the decoherence and the periodic driving. If, for example, the period T is much larger than the inverse dephasing rates, the shuttle mechanism is expected to be inefficient and the critical current is strongly suppressed. In the following we will describe a quite rich scenario, depending on the relative value of the various time scales and phase shifts.

As charge is conserved by the coupling to the environment, $[\hat{n}, \hat{H}_{int}] = 0$, current can flow only trough the electrodes. Therefore, in the Heisenberg picture, $\hat{I}_L(t) + \hat{I}_R(t) + \dot{\hat{n}} = 0$. By integrating over a period the average current reads ($I_R = -I_L \equiv I$)

$$I = \text{Tr} \{ \hat{n}(\rho(t_L) - \rho(0)) \} = \text{Tr} \{ \hat{n}(\rho(T/2) - \rho(0)) \}.$$

We set the initial time within a period at the beginning of contact with the left lead.

Using the steady state density matrix Eq.(14) we can derive a formal expression for the DC Josephson current in the system:

$$I = \frac{e}{T} \mathbf{z} \cdot [(\mathbf{I} - M_0)^{-1} \mathbf{v}_0 - \mathbf{z} \cdot (\mathbf{I} - M_{T/2})^{-1} \mathbf{v}_{T/2}] \quad (23)$$

$$M_0 = \exp(G_{\leftarrow} t_{\leftarrow}) \cdot R(\chi_{\leftarrow}) \cdot \exp(G_R t_R) \cdot \exp(G_{\rightarrow} t_{\rightarrow}) \cdot R(\chi_{\rightarrow}) \cdot \exp(G_L t_L) \quad (24)$$

$$\mathbf{v}_0 = -2 \exp(G_{\leftarrow} t_{\leftarrow}) \cdot R(\chi_{\leftarrow}) \cdot [\gamma_R G_R^{-1} \cdot (\mathbf{I} - \exp(G_R t_R)) \mathbf{w}_R + \gamma_L \exp(G_R t_R) \cdot \exp(G_{\rightarrow} t_{\rightarrow}) \cdot R(\chi_{\rightarrow}) \cdot G_L^{-1} \cdot (\mathbf{I} - \exp(G_L t_L)) \mathbf{w}_L] , \quad (25)$$

and $M_{T/2}$, $\mathbf{v}_{T/2}$ are obtained from M_0 , \mathbf{v}_0 by the exchange of right and left Josephson contacts and of forward and backward free evolution time. This means that $M_{T/2} = \mathcal{P} M_0$, $\mathbf{v}_{T/2} = \mathcal{P} \mathbf{v}_0$ with \mathcal{P} acting on the parameters $\theta_{L(R)}$, $\chi_{\rightarrow(\leftarrow)}$, $\gamma_{L(R)} t_{L(R)}$, $\gamma_{\rightarrow(\leftarrow)} t_{\rightarrow(\leftarrow)}$, $\phi_{L(R)}$ as:

$$\mathcal{P} : (L, \rightarrow, R, \leftarrow) \Rightarrow (R, \leftarrow, L, \rightarrow) . \quad (26)$$

The expression of the current, which depends on all the previous parameters can be obtained analytically from Eq.(23) by explicitly writing M_0 and \mathbf{v}_0 in terms of the various parameters. The current depends only on the phase difference between the two superconductors $\phi_R - \phi_L$. It is an odd function with respect to the action of \mathcal{P} defined by Eq. (26). From this observation follows that, even for $\phi = 0$, there can be a supercurrent between the leads as long as the evolution over a cycle is not \mathcal{P} -invariant. In this sense the system behaves like a non-adiabatic Cooper pair pump.

The main features of the Josephson current in the Cooper pair shuttle have been discussed in Ref. 11 and we recall them here for completeness however providing a number of new results and additional details. In the

where \mathbf{z} is the unitary vector $(0, 0, 1)^T$, \cdot stands for the usual scalar product in \mathbb{R}^3 , and $M_{T/2}$, $\mathbf{v}_{T/2}$, M_0 , \mathbf{v}_0 are defined in Eq. (12). Their explicit form is

case of $\theta_L = \theta_R = \theta$, $\chi_{\rightarrow} = \chi_{\leftarrow} = \chi$, $\gamma_L = \gamma_R = \gamma_J$, $\gamma_{\rightarrow} = \gamma_{\leftarrow} = \gamma_C$, $t_L = t_R = t_J$, $t_{\rightarrow} = t_{\leftarrow} = t_C$, Fig. 3 shows a typical plot of I as a function of θ and ϕ . Depending on the value of θ (a similar behavior is observed as a function of χ), the critical current can be negative, i.e. the system can behave as a π -junction. The current dependence on the various phases is the result of the interference between different path corresponding to different time evolutions for the charge states in the grain. By changing $\gamma_J t_J$ and $\gamma_C t_C$, certain interference paths are suppressed, resulting in a shift of the interference pattern and ultimately in a change of the sign of the current, as shown in Fig.3.

Another interesting aspect of the Josephson current is that it is a non-monotonous function of $\gamma_J t_J$, i.e. by *increasing* the damping, the Josephson current can *increase*. The behavior as a function of the dephasing rates is presented in Fig.3. The presence of a maximum Josephson current at a finite value of $\gamma_J t_J$ can be understood by noting that the current is vanishing in the strong and weak damping limits. In both the limits simple analytic expressions are available.

If the dephasing is strong, I can be expanded in powers of $e^{-\gamma_L t_L + \gamma_{\leftarrow} t_{\leftarrow}}$ and $e^{-\gamma_{\rightarrow} t_{\rightarrow} + \gamma_R t_R}$ and, to leading order,

$$I \sim \frac{2e}{T} \left[\tanh\left(\frac{E_L}{T_b}\right) e^{-(\gamma_L t_L + \gamma_{\leftarrow} t_{\leftarrow})} \sin(2\theta_L) \sin(\phi - \chi_{\leftarrow}) + \tanh\left(\frac{E_R}{T_b}\right) e^{-(\gamma_R t_R + \gamma_{\rightarrow} t_{\rightarrow})} \sin(2\theta_R) \sin(\phi + \chi_{\rightarrow}) \right] . \quad (27)$$

For simplicity we assume that the Josephson energies at left and right contacts are equal, as well as the contact and free evolution time. In this case the previous expression is simplified to

$$I_{strong} \sim \frac{2e}{T} \tanh\left(\frac{E_J}{T_b}\right) e^{-(\gamma_J t_J + \gamma_C t_C)} \cos(\chi_{\rightarrow} + \chi_{\leftarrow}) \sin(2\theta) \sin(\phi + (\chi_{\rightarrow} - \chi_{\leftarrow})) . \quad (28)$$

It is worth to notice the presence of a net DC current even in the case of $\phi = 0$ as argued from general argument presented before. The role of breaking the \mathcal{P} -invariance

is then played by the difference of the dynamical phases accumulated in the forward and backward free evolution time intervals, $\chi_{\rightarrow} - \chi_{\leftarrow}$. If instead we assume a perfect

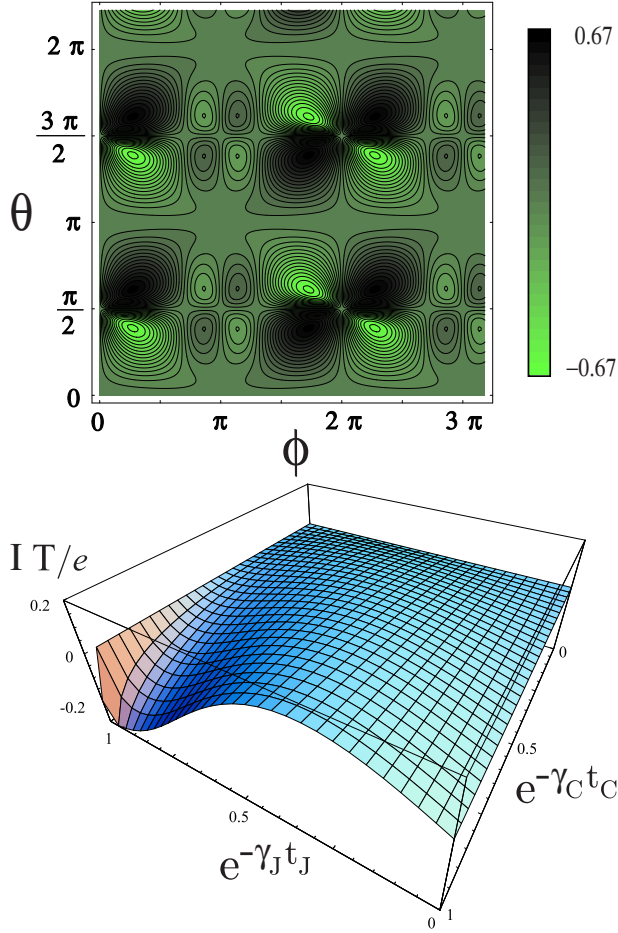


Figure 3: Upper panel. Supercurrent (in units of e/T) as a function of the superconductor phase difference ϕ and of the phase accumulated during the contact to one of the electrodes θ . The other parameters are fixed as: $\chi = 5\pi/6$, $e^{-\gamma_J t_J} = 3/4$, $e^{-\gamma_C t_C} = 4/5$. The plot is obtained for $T_b \ll E_J$. Lower panel. Average current ($T_b \ll E_J$) as a function of the dephasing rates, with $\phi = -3\pi/4$, $\theta = 7\pi/10$, $\chi = 5\pi/6$. As a function of $\gamma_J t_J$, the supercurrent has a non-monotonous behavior. Note the change of sign in the current obtained by varying decoherence rates in each time interval separately.

\mathcal{P} -invariance, we recover the known expression for the DC current of Ref. 11

$$I_{strong} \sim \frac{2e}{T} \tanh\left(\frac{E_J}{T_b}\right) e^{-(\gamma_J t_J + \gamma_C t_C)} \cos(2\chi) \sin(2\theta) \sin\phi. \quad (29)$$

Strong dephasing is reflected in the simple (*i.e.* $\propto \sin\phi$) current-phase relationship and in the exponential suppression of the current itself. Strong dephasing, in fact, suppresses coherent transport over multiple cycles, thus giving a corresponding suppression of higher harmonics in the current-phase relationship, *i.e.* a suppression of terms $\propto \sin^{2m+1}(\phi)$, $m \in \mathbb{N}$.

For the sake of simplicity, from now on, we present all the result in the case of perfect \mathcal{P} -invariance of the time evolution of the density matrix in a period. This is not a serious limitation for the experimental setups.

In the opposite limit of weak damping defined by $\gamma_J t_J \ll \gamma_C t_C \ll 1$

$$I_{weak} \sim \frac{2e}{T} \tanh\left(\frac{E_J}{T_b}\right) \frac{\gamma_J t_J}{\gamma_C t_C} \frac{(\cos\phi + \cos 2\chi) \tan\theta \sin\phi}{1 + \cos\phi \cos 2\chi}. \quad (30)$$

The current tends to zero if the coupling with the bath is negligible during the contact time. In this case the time evolution in the intervals L, R is almost unitary, while, in the region C , pure dephasing leads to a suppression of the off-diagonal terms of the reduced density matrix $\rho(t)$. As a result, in the stationary limit the system is described by a complete mixture with equal weights. At the point $(\gamma_J t_J, \gamma_C t_C) = (0, 0)$ our model is not defined as discussed at the end of Section III. The limiting value of the current in approaching such point depends on the relative strength $\gamma_J t_J \lesseqgtr \gamma_C t_C$ between this two parameters.

The current tends to zero in both limiting cases of large and small $\gamma_J t_J$. Therefore one should expect an optimal coupling to the environment where the Josephson current is maximum. A regime where the crossover between the strong and weak damping cases can be described in simple terms is the limit $\gamma_C \rightarrow 0$, for a fixed value of θ . For example, at $\theta = \pi/4$ the current reads

$$I = \frac{2e}{T} \tanh\left(\frac{E_J}{T_b}\right) \frac{2e^{-\gamma_J t_J} [2e^{-2\gamma_J t_J} \cos\phi + (1 + e^{-4\gamma_J t_J}) \cos 2\chi] \sin\phi}{(1 + e^{-2\gamma_J t_J})(1 + e^{-2\gamma_J t_J} \cos\phi \cos 2\chi + e^{-4\gamma_J t_J})} \quad (31)$$

In the limit of vanishing $\gamma_J t_J$, Eq.(31) corresponds to the situation discussed in Ref. 9. Indeed, both expressions are independent of the dephasing rates. The difference in the details of the current-phase(s) relationship are due to the different environment.

In all the three cases presented here, Eqs.(29, 30, 31), the change of sign of the current as a function of the phase shifts θ or χ is present.

D. Effect of driving fluctuations

The expressions for the current, discussed in the previous Section, depend on the specific form of the coupling between the system and the reservoir. The decoherence we considered so far originates from gate voltage fluctuations. In addition in the shuttling mechanism an unavoidable coupling to an environment producing fluctuations in the period and shape of the driving is also present. We are therefore interested also in considering the effect of fluctuations in the time dependence of the external parameters on the Josephson current. Having assumed a step-like time dependence of the parameters of the Hamiltonian, noise in the external driving consists in fluctuations of the switching times. This means that the contact times t_L , t_R and the free evolution times t_{\rightarrow} , t_{\leftarrow} take, at any cycle i , a random value $t_b(i)$, $b = L, R, \rightarrow, \leftarrow$. It is reasonable to assume that the fluctuations of any switching time are independent on the others. In terms of

time intervals $t_b(i)$, it follows that the fluctuations $\Delta t_b(i)$ around the average value t_b , are uncorrelated at different periods. Within the same period the fluctuations of any two distinct time intervals are also independent. Hence

$$\langle \Delta t_b(i) \rangle_t = 0 \quad (32)$$

and

$$\langle (\Delta t_a(i))^n (\Delta t_b(j))^m \rangle_t = \langle (\Delta t_a(i))^n \rangle_t \langle (\Delta t_b(j))^m \rangle_t \quad (33)$$

if $i \neq j \vee a \neq b$. The integer valued arguments of $\Delta t_b(\cdot)$ labels the periods and the subscript index runs over the set $L, R, \rightarrow, \leftarrow$. The average on the stochastic process is defined by $\langle \cdot \rangle_t$. We will discuss later the distribution function of $\Delta t_b(i)$.

By using the same notation in Eq. (11), we can write the evolution of the density matrix after a finite number of cycles, $h \geq 1$, as

$$\mathbf{r}(t + \sum_{k=1}^h T(k)) = \prod_{\lambda=0}^{h-1} M_t(\lambda) \mathbf{r}(t) + \sum_{\lambda=0}^{h-2} \prod_{\mu=\lambda}^{h-2} M_t(\lambda + \mu + 1) \mathbf{v}_t(\lambda) + \mathbf{v}_t(h-1). \quad (34)$$

In the previous equation the expressions $M_t(i)$ and $\mathbf{v}_t(i)$ are those defined in Eq. (11). The index in parenthesis indicates the explicit dependence of both M_t and \mathbf{v}_t on various $t_b(i)$. We refer to $T(k) = \sum_b t_b(k)$ as the period although the time evolution is no longer periodic (before averaging); $T(k)$ is in fact the time the shuttle takes to complete a cycle, k labels the number of cycles. The first term in the right-hand-side of Eq. (34) vanishes in the long-time limit $h \rightarrow \infty$. Averaging the previous expression over the fluctuations of the switching times according to Eq. (33) is straightforward, leading to

$$\langle \mathbf{r}_\infty(s) \rangle_t = (\mathbf{1} - \langle M_s \rangle_t)^{-1} \langle \mathbf{v}_s \rangle_t. \quad (35)$$

Note that if we had considered only the external driving fluctuations (*i.e.* neglecting the effect of gate voltage fluctuations) we would have found, in the steady state,

$\rho_\infty(t) \propto \mathbf{1}$. In this case in fact the evolution of $\mathbf{r}(t)$ consists in an alternate sequence of rotation on the Bloch sphere around the $(1, 0, 0)$ and $(0, 0, 1)$ axes. Due to uncertainty in the rotation angles it is a random walk which leads, at long time, to a uniform distribution over the Bloch sphere. The nontrivial result in Eq. (35) arises because of the interplay between the two stochastic processes of gate voltage fluctuations and switching time fluctuations. They are independent because there is a time scale separation between these two processes: Correlations in the quantum bath do occur on a time scale $\tau_c \ll T$, while the time intervals $t_b(i)$ do not fluctuate within any single cycle.

We are interested in averaging the current after the system has reached its steady state

$$\langle I \rangle_t = \lim_{N \rightarrow \infty} \left\langle \frac{2e}{\sum_{i=1}^N T(i)} \text{Tr} \left[\hat{n} \sum_{j=1}^N \left(\mathcal{M}_{0 \rightarrow \sum_{h=1}^{j-1} T(h) + t_L(j)} - \mathcal{M}_{0 \rightarrow \sum_{h=1}^{j-1} T(h)} \right) [\rho(0)] \right] \right\rangle_t, \quad (36)$$

In order to proceed further we need to specify the distribution function $P(\Delta t_b(i))$. Let us note that the distribution is meaningful only if $P(\Delta t_b(i)) = 0$ for $\Delta t_b(i) < 0$.

We consider

$$P(\Delta t_b(i)) = \theta(\Delta t_b(i) + \tau) \theta(\tau - \Delta t_b(i)) / 2\tau, \quad (37)$$

with $\tau < t_b \forall b$ as a toy model: the underlying physical idea is that the switching time can be controlled with a precision 2τ and the switching can happen with equal probability in the interval $[t_b - \tau, t_b + \tau]$ ⁴⁸. We do not expect that this simple form of the distribution function can determine the quantitative details of the Josephson current, rather it can grasp the main features of physical effects due to imprecision in controlling the external

driving. For the sake of concreteness, let us consider the limit of strong dephasing (Eq. (29)), when the expression for the current considerably simplifies. The strong dephasing leads to a rapid loss of memory of the initial conditions. One can suppose that this occurs after one cycle independently on the averaging process. It follows that, in Eq. (36),

$$\langle I \rangle_t = \lim_{N \rightarrow \infty} \left\langle \frac{2e}{\sum_{i=1}^N T(i)} \text{Tr} \left[\hat{n} \sum_{j=1}^N \left(\mathcal{M}_{\sum_{h=1}^{j-1} T(h) \rightarrow \sum_{h=1}^{j-1} T(h) + t_L(j)} - \mathbb{1} \right) [\rho_\infty(0)] \right] \right\rangle_t, \quad (38)$$

\mathcal{M} depends only on the stochastic parameters of the last ($= j$ th) cycle and $\rho_\infty(0)$ on parameters of the $j - 1$ th cycle. By considering the expansion of the denominator in the previous equation as

$$1/\left(\sum_{i=1}^N T(i)\right) = 1/(NT)(1 - \sum_{i=1}^N \sum_b \Delta t_b(i)/NT + \dots) \quad (39)$$

together with Eq. (33), Eq. (36) reduces to

$$\langle I \rangle_t = \lim_{N \rightarrow \infty} \frac{2e}{NT} \left\langle \text{Tr} \left[\hat{n} \sum_{j=1}^N \left(\mathcal{M}_{\sum_{h=1}^{j-1} T(h) \rightarrow \sum_{h=1}^{j-1} T(h) + t_L(j)} - \mathbb{1} \right) [\rho_\infty(0)] \right] \right\rangle_t + \mathcal{O}(1/N). \quad (40)$$

In the $N \rightarrow \infty$ limit, only the first term in the previous equation is non-vanishing. It means that, as a consequence of the strong dephasing, the effect of fluctuations in the term $1/T$ in the definition of the current are ineffective. The final expression for the average current is

$$\langle I \rangle_t = \frac{2e}{T} \sin \phi \left\langle e^{-\gamma_C t} \cos \frac{E_C t}{\hbar} \right\rangle_t \left\langle e^{-\gamma_J t_L} \sin \frac{E_J t_L}{\hbar} \right\rangle_t \quad (41)$$

which, in the lowest orders in the small parameter $\tau E_C/\hbar$, reads

$$\langle I \rangle_t \approx \frac{2e}{T} \left\{ \left[1 - \frac{1}{6} \left(\frac{E_C \tau}{\hbar} \right)^2 \right] I_{strong} + \frac{1}{3} \left(\frac{E_C \tau}{\hbar} \right)^2 \left[\frac{\hbar \gamma_C}{E_C} \times \sin(2\theta) \sin(2\chi) - \frac{E_J}{E_C} \frac{\hbar \gamma_J}{E_C} \cos(2\theta) \cos(2\chi) \right] \sin \phi \right\}, \quad (42)$$

with the further condition $1/T \ll \gamma_J \ll E_J/\hbar \ll E_C/\hbar \gg \gamma_C \gg 1/T$. The current I_{strong} is defined as the current in absence of driving fluctuations and is that obtained in Eq. (29). The leading order correction to I_{strong} does not modify the functional dependence of the current on the dynamical phases: It is a simple renormalization of the pre-factor, $1 \rightarrow 1 - (E_C \tau)^2/(6\hbar^2)$. Eq. (42) shows that higher order corrections can instead lead to a modifications of the functional dependence of the current on dynamical phases.

E. AC Josephson effect

When a bias voltage is applied to a Josephson junction it results in an alternating current. This is the AC

Josephson effect which can be derived from the expression for the Josephson current $I = \frac{2e}{\hbar} E_J \sin(\phi_R - \phi_L)$ supplemented by the Josephson relation $\frac{d}{dt}(\phi_R - \phi_L) = \frac{2e}{\hbar} V$. In the present problem the alternating current will not be simply sinusoidal, it is therefore convenient to consider its frequency spectrum defined as

$$\tilde{I}(\omega) = \int_{\mathbb{R}} dt e^{-i\omega t} \langle I \rangle(t). \quad (43)$$

(in the simple case of a sinusoidal current it reads $\tilde{I}(\omega) \propto \delta(\omega - 2eV/\hbar)$ for $\omega > 0$).

The application of a finite voltage bias in the Cooper pair shuttle gives rise to a quite rich situation, due to the interplay of the voltage bias effect and the underlying periodic motion of the shuttle. The relative magnitude

of the characteristic frequencies, $\sim 2eV/\hbar$ and $\sim 1/T$, determine different regimes that we are going to investigate.

We set the electric voltage of the left and right electrode respectively equal to $V_L = -V/2$ and $V_R = V/2$. There is no dissipative current through the system as long as $eV \ll 2\Delta$. In the limit $C_L, C_R \lesssim C_g$, and $(V/2) \ll V_g$ the Hamiltonian of the system is still given by Eq. (1). The effect of the electric potential $V_{L(R)}$ in the two leads can be included, by means of a gauge transformation, into time dependent phases of the condensate wave functions, $|\psi_{L(R)}\rangle \rightarrow e^{2ieV_{L(R)}t/\hbar} |\psi_{L(R)}\rangle$, or equivalently,

$$\phi_{L(R)} \rightarrow \phi_{L(R)} + 2eV_{L(R)}t/\hbar.$$

The Hamiltonian describing the effect of voltage bias in the Cooper pair shuttle becomes

$$\begin{aligned} \hat{H}_{AC} &= E_C(t)[\hat{n} - n_g(t)]^2 \\ &- E_J\Theta_L(t)\cos(\hat{\varphi} - \phi_L - eVt/\hbar) \\ &- E_J\Theta_R(t)\cos(\hat{\varphi} - \phi_R + eVt/\hbar). \end{aligned} \quad (44)$$

We are interested in the frequency dependent current

$$\begin{aligned} \tilde{I}(\omega) &= 2e\frac{E_J}{\hbar} \int_{\mathbb{R}} dt e^{-i\omega t} \Theta_L(t) \mathcal{I}(t) \\ &= 2e\frac{E_J}{\hbar} \sum_{k \in \mathbb{Z}} e^{-ik\omega T} \int_0^{t_L} ds e^{-i\omega s} \mathcal{I}(s + kT) \end{aligned} \quad (45)$$

where $\mathcal{I}(t) = \text{Tr} \{ \sin(\hat{\varphi} - \phi_L - eVt/\hbar) \rho(t) \}$, according to the definition of current in Eq. (5).

We computed numerically the time evolution of the density matrix of the island and obtained from it the frequency spectrum of the Josephson current. As a warm up we consider the simplest case which consists in neglecting the effect of voltage bias. This is the same case considered in previous Sections, in which, however, we analyze the instantaneous current rather than the averaged one. The results are presented in Fig 4. The spectrum clearly signals the periodicity of the time dependence of the current signal and of the presence of the Θ_L function. In the steady state the current is repeats periodically and then $\mathcal{I}(s + kT) = \mathcal{I}(s)$ in Eq. (45). As a consequence the current spectrum presents peaks at integer multiples of the frequency $\omega_n = 2\pi/T$,

$$\tilde{I}(\omega) = \sum_n \tilde{A}_n \delta(\omega - 2\pi n/T) \quad (46)$$

with

$$\tilde{A}_n = \int_0^{t_J} ds \exp(-2\pi i n s/T) \mathcal{I}(s).$$

The form of \tilde{A}_n is fixed by the expression of the density matrix at the fixed point through $\mathcal{I}(s)$, $\mathcal{I}(s) = \mathbf{y} \cdot \mathbf{R}_z(\phi_L) \mathbf{r}(s)$, and with $\mathbf{r}(s)$ determined by Eq. (18). The signal $\mathcal{I}(s)$ consists of damped oscillations at frequency E_J/\hbar , $\mathcal{I}(s) \propto \exp(-\gamma_J s) \sin(E_J s/\hbar + \alpha_0)$. The Fourier

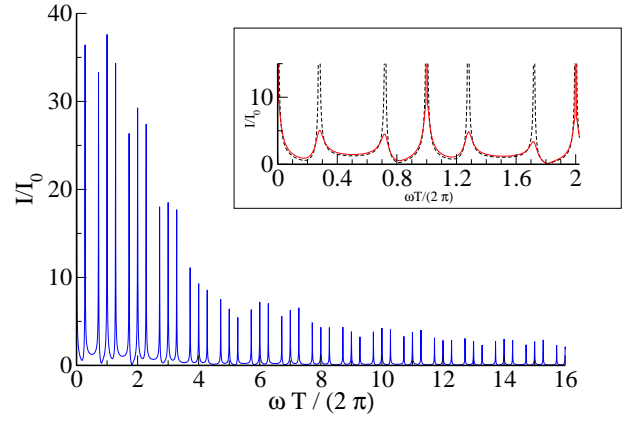


Figure 4: Absolute value of the Fourier transform of the Josephson current in units of $I_0 = 2eE_J/\hbar$. The plot is obtained for $t_J = t_C = T/4$, $E_C T/\hbar = 60$, $E_J T/\hbar = 6$, $\gamma_J T = \gamma_C T = 0.001$. In the inset we plot the Fourier transform of the Josephson current in a restricted range of frequencies for $\gamma_J T = \gamma_C T = 0.001$ (black dotted line) and for $\gamma_J T = \gamma_C T = 0.1$ (full red line).

transform of such a signal determines the characteristic features of the current spectrum presented in Fig. 4. Now $|\tilde{A}_n|$ displays oscillations at frequencies T/t_J modulated by a power-law decay function ($\propto 1/\omega$, for $\omega \gg E_J/\hbar$). The nature of the other peaks shown in the inset in Fig. 4 is completely different, in fact they are strongly suppressed by the presence of decoherence. We can describe the mechanism that originates these peaks if the decoherence is absent. In this case any component of the density matrix is an oscillatory function with frequency E_J/\hbar , E_C/\hbar at contact or free evolution interval respectively. The matching between these two different functions at the boundary between consecutive time intervals determines the phase α_k in the expression for $\mathcal{I}(s)$ after k periods. We get $\mathcal{I}(s) \propto \sin(E_J s/\hbar + kT(E_C - E_J)/(2\hbar))$. Substituting this expression into Eq. (45), we find the existence of peaks in the frequency spectrum of the current at $\omega = (2\pi/T)(k \pm (E_C - E_J)/4\pi\hbar)$, $k \in \mathbb{Z}$, as presented in Fig. 4. The stronger decoherence is, the more suppressed such peaks are.

This picture is modified in presence of a finite voltage bias between the two superconductors, as presented in Fig. 5. The features of the frequency spectrum in this case depends on whether the condition $2eV \ll \hbar/T$ or $2eV \gg \hbar/T$ is fulfilled. For small V , one can suppose that the system reaches a steady state which evolves in time only through the time dependence of the parameter $\phi \rightarrow \phi + 2eVT/\hbar$. It means we can replace $\mathcal{I}(s + kT) \sim \sin(E_J s/\hbar + 2eV kT/\hbar)$. In this regime the spectrum exhibits a splitting of the frequencies of the peaks $\omega = (2\pi/T)(k \pm eVT/(\pi\hbar))$. This is shown in the upper panel in Fig. 5 for $k = 1$, the peak at lowest frequency. The effect the peaks at higher frequencies is the same, therefore we focus on the first peak at $\omega = 2\pi/T$

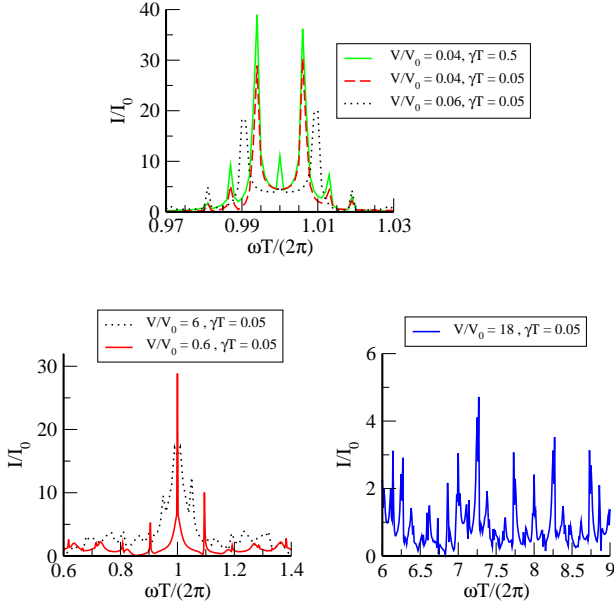


Figure 5: Absolute value of the Fourier transform of the Josephson current (all panels) in units of $I_0 = 2eE_J/\hbar$ in the different regimes: $eVT/\hbar \ll 1$ (upper panel), $eVT/\hbar \simeq 1$ (lower left panel), $eVT/\hbar \gg 1$ (lower right panel). The plots are obtained for $t_J = t_C = T/4$, $E_C T/\hbar = 60$, $E_J T/\hbar = 6$. The values of V , in units of $V_0 = \hbar/(2eT)$, and $\gamma_J = \gamma_C = \gamma$ for the various plots are indicated in the legends.

since it is the most pronounced (the values at the peaks \tilde{A}_n decays with increasing the frequency as in the case $V = 0$, see Fig. 4). Fig. 5 also shows the presence of other peaks at integer multiples of $2eV/\hbar$ which cannot be interpreted within the simple model just presented. Moreover the width of the peaks is weakly dependent on $\gamma_{J(C)}$. The presence of higher harmonics in the spectrum becomes evident for $\hbar/2eV \sim T$ (see lower left panel in Fig. 5). The presence of higher harmonics, although we do not have a detailed simple explanation, is expected once we write the Josephson coupling in the Hamiltonian Eq. (44) as $E_J \cos(\phi - 2eV/\hbar) \cos(\hat{\varphi} + (\phi_L + \phi_R)/2)$. This shows that E_J is modulated by an oscillatory time dependent factor. Even if further complicated by the presence of time order operator in the time evolution operator, the current $\mathcal{I}(s + kT)$ would present terms $\propto \sin(E_J \cos(2eV(s + Kt)/\hbar))$ which generates all the harmonics. In the voltage dominating regime $2eV/\hbar \gg 1/T$, the spectrum does not display new effects apart from the described V -splitting and an enhancement of peaks corresponding to high harmonics (lower right panel in Fig. 5).

IV. THE CHAOTIC REGIME OF COOPER PAIR SHUTTLING

Up to now we have discussed the properties of the Cooper pair shuttle in the limit of small Josephson cou-

pling, $E_J \ll E_C$. In this Section we consider the opposite regime, $E_J \gg E_C$. If the external time-dependent driving were absent, such limit would not be of great interest: It simply corresponds to a SSET in the Josephson dominate regime, whose physics is already known³. Due to the time dependence of the Josephson couplings in the Cooper pair shuttle, instead, there is a time lapse in which the Josephson energy is vanishing (see Fig. 1), and therefore the charging effects still play a leading role.

We will show that the dynamics of the Cooper pair shuttle mimics that of a Quantum Kicked Rotator (QKR) with the additional free parameter, ϕ . The kicked rotator is a chaotic system in the classical limit. In the quantum regime it presents a variety of interesting phenomena, including dynamical localization²³. Despite the long-standing interest in the QKR, only few proposals have been put forward and the only experimental implementation so far has been realized with cold atoms exposed to time-dependent standing waves of light^{24,25,26}. The Cooper pair shuttle can therefore provide a remarkable implementation of the QKR¹³ by means of superconducting nanocircuits⁴⁹. This allows us to study the effects of dynamical localization on the transport properties of a mesoscopic device. So far the effect of dynamical localization on the current in a mesoscopic systems has been discussed only in Ref. 27 for a quantum dot under ac pumping in which it affects the shape of Coulomb blockade peaks.

A. From classical to quantum dynamics in the chaotic Cooper pair shuttle

We start our analysis from the Hamiltonian in Eq. (1) which is valid irrespective of the relative strength between E_C and E_J . For sake of simplicity we assume $n_g = 0$ throughout this section, thus rewriting Eq. (1) as

$$\hat{H}_0 = E_C \hat{n}^2 - E_J \sum_{n \in \mathbb{N}} [\cos(\varphi - \phi_L) \Theta(t - nT) + \cos(\varphi - \phi_R) \Theta(t - (2n + 1)T/2)], \quad (47)$$

where $\Theta(t) = \theta(t)\theta(t_J - t)$ having assumed the simple limit $t_L = t_R = t_J$, $t_{\rightarrow} = t_{\leftarrow} = t_C$. The dynamics of the Cooper pair shuttle reduces to that of a QKR when the contacts times are short enough to neglect the effects of charging energy. In this case the time evolution operator during the Josephson contact is $\exp[-iE_J t_J \cos(\hat{\varphi} - \phi_{L,R})/\hbar]$. In the rest of the cycle the shuttle evolves according to the charging Hamiltonian only. Let us explain this in some detail. Because we are interested in the dynamics of the system at long time compared with the period T , any physical observable, as already noted in Section III, is determined by the density matrix at integer multiples of the period and therefore by the Floquet operator which is the time evolution operator over a period. Under the assumption that $E_J \gg E_C$,

if E_C cannot induce a significant change of φ during the Josephson contact, the Floquet operator becomes

$$\hat{U}(T, 0) = \hat{J}_R \hat{V} \hat{J}_L \hat{V} \quad (48)$$

where \hat{J} and \hat{V} are the time evolution operators respectively during the Josephson contacts and the free evolution times

$$\hat{J}_{R,L} = e^{-ik \cos(\hat{\varphi} - \phi_{L,R})}, \hat{V} = e^{-i\frac{K}{2\hbar} \hat{n}^2}, \quad (49)$$

where

$$k = E_J t_J / \hbar \quad \text{and} \quad K = (2E_C t_C / \hbar)(E_J t_J / \hbar).$$

The condition that the superconducting phase difference is left unchanged at the contacts reads $n E_C t_J / \hbar \lesssim 1^{28}$, thus establishing a condition on the maximum number of allowed charge states involved in the dynamics. This condition is essentially independent on the exact time dependence of $E_J(t)$. The Floquet operator in Eq. (48) is the same of the Quantum Kicked Rotator (QKR) with the additional parameter $\phi = \phi_R - \phi_L$. This shows that the physics of the Cooper pair shuttle, in the limit $E_J \gg E_C$, may reproduce that of the QKR, and, for $\phi \neq 0$, provides an interesting generalization.

The kicked rotator is the first model in which characteristic quantum effects of classically chaotic system have been observed numerically^{23,29}. As the parameters k, K in Eq. (48) are varied, the dynamics of the QKR exhibits several appealing phenomena, including quantum ergodicity, quantum resonances and dynamical localization²³. For a discussion about classically chaotic system and various characteristic features of their quantum version we refer to the literature (see Ref. 23. and references therein). Here we note that the exponential localization of the wave function due to interference effects is one of the most relevant of the mentioned features. The dynamics of the quantum kicked rotator follows the classical exponential instability (characterized by a positive Lyapunov exponent λ) up to the Ehrenfest time t_E ³⁰. This sets the time scale at which quantum interference effects starts to be important leading to weak localization correction to the classical behavior³¹. After a localization time t^* the classical-like diffusive behavior is suppressed by quantum effects^{23,29}. Since typically $t^* \gg t_E$, the diffusive behavior is possible also in the absence of exponential instability.

The Floquet operator in Eq. (48) can be written through the redefinition $\hat{p} = (K/k)\hat{n}$ in terms of

$$\hat{V}' = \exp(-i\hat{p}^2/2\hbar\tilde{k}) \quad (50)$$

$$\hat{J}'_{L(R)} = \exp[-iK \cos(\varphi - \phi_{L(R)})/\hbar\tilde{k}], \quad (51)$$

so that $\hat{U}(T, 0)$ depends only on K , while $[\hat{p}, \hat{\varphi}] = -i\hbar K/k = -i\hbar\tilde{k}$; \tilde{k} plays the role of an effective Planck constant. The classical limit is therefore obtained for $k \rightarrow \infty$ (or equivalently $\tilde{k} \rightarrow 0$), keeping $K = \text{const}$ and the classical dynamics depends only on the parameters K and $\phi = \phi_R - \phi_L$.

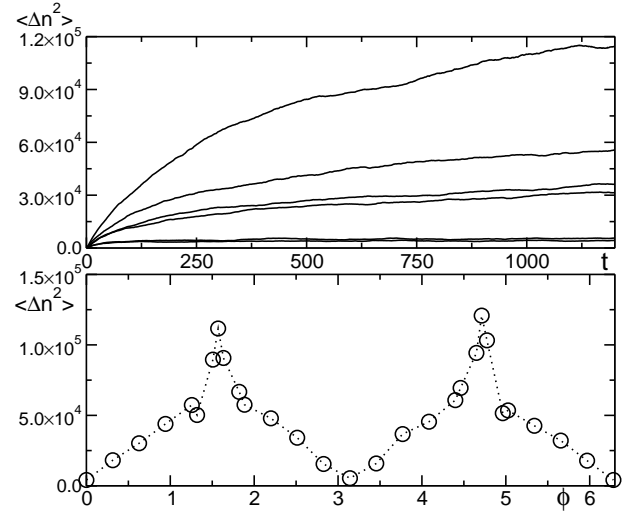


Figure 6: Upper panel. $\langle (\Delta n)^2 \rangle = \langle (n - \langle n \rangle)^2 \rangle$ as a function of time for $K = 10$, $k = 15$, and phase difference (from bottom to top) $\phi/(2\pi) = 0, 0.05, 0.1, 0.4, 0.8, 0.25$. Lower panel. Saturation value of $\langle (\Delta n)^2 \rangle \propto \ell^2$ as a function of ϕ for the same parameter values as in the upper panel.

In the classical limit the equations of motion of the Cooper pair shuttle correspond to a slightly modified Chirikov map

$$\begin{cases} p_t = p_{t-1} - K \sin\{\theta_{t-1} - [(t+1) \bmod 2]\phi\} \\ \theta_t = \theta_{t-1} + p_t, \end{cases} \quad (52)$$

with $\theta = \varphi - \phi_L$ and where subscripts label the number of contacts with the leads (kicks). The dynamics of a given distribution function in the phase space under the action of the Chirikov map at $\phi = 0$ is known: For $K > 1$, the angular variable θ is uniformly spread over $[0, 2\pi]$ after few kicks; p follows a diffusive behavior. The role of ϕ in the classical map can be investigated by following Ref. 32. The idea is to substitute the deterministic description in Eq. (52) with a probabilistic one where a random term $\delta\theta_t$ is added to the second equation of (52). We obtain a diffusive dynamics for the charge on the central island for $K > 1$ (details of the calculation are in Appendix B): $\langle (n_t - n_0)^2 \rangle \xrightarrow{t \rightarrow \infty} 2Dt$, with t measured in integers multiples of the period and where D is the diffusion coefficient

$$D = \frac{k^2}{2} \left[1 - 2 \cos(2\phi) J_2(K) + \mathcal{O}\left(\frac{1}{K}\right) \right]. \quad (53)$$

The QKR follows the classical diffusive behavior up to the localization time t^* . Quantum interference effects, as shown in Fig. IV A (upper panel), for $t > t^*$, suppress this chaotic diffusion: The wave function is exponentially localized in the charge basis, over a localization length ℓ , and we have $\ell \sim t^* \sim D^{23}$.

The charge fluctuations of the central island freeze in time. The localization length can be further tuned by changing the phase difference as demonstrated in the

lower panel of Fig. IV A. Such quantum effects have not yet found a complete analytic explanation. An important step into the problem has recently been achieved by Tian, Kamenev and Larkin³¹. They calculated the quantum corrections at time $t \gtrsim t_E$ where such corrections are small (but nonanalytic) in \hbar . From their approach it is clear that the presence of ϕ , by breaking the time reversal symmetry in the system, does affect quantitatively the quantum corrections to localization.

B. Time reversal symmetry breaking - COE to CUE crossover

Although the diagrammatic approach discussed in Ref. 31 shades light on the role of the phase difference in the system, it cannot give quantitative predictions on the fully localized state at long time. We are interested in discussing the effect of ϕ in the localized state. The breaking of TRS by the superconducting phase difference, ϕ , can be seen by direct verification that the Floquet operator in Eq. (48) at $\phi = 0$ is invariant under the action of

$$T : \begin{cases} t \rightarrow -t \\ n \rightarrow n \\ \varphi \rightarrow -\varphi \end{cases}, \quad (54)$$

while such symmetry is broken at $\phi \neq 0$.

In the analogous problem of localization in disordered metals, it is known that the TRS breaking results in a reduction by a factor 1/2 of the the weak localization corrections and in a doubling of the localization length (see Ref. 33). The same kind of effects have been observed in chaotic systems as well³⁴. In fact, we also observe a doubling of localization length at $\phi = \pi/2$ with respect to the $\phi = 0$ case as shown in Fig. IV A. Note that the effect of doubling of the localization length has to be added to the effect of variation of the localization length through the change in the classical diffusion coefficient in Eq. (53).

The effect of TRS breaking can be further investigated by looking at the distribution of quasienergies spacing. The reason behind this is the conjecture that quantum properties of classically chaotic systems are well described by the Random Matrix Theory (RMT)³⁵. This has been shown to hold for a wide class of chaotic systems³⁶ (though exceptions exist³⁷). In the RMT the breaking of the time reversal symmetry consists in a crossover from the Circular Orthogonal Ensemble (COE) to the Circular Unitary Ensemble (CUE) for the Floquet operator.

In order to check this conjecture we look at the level spacing probability distribution function $P(s)$ of the quasienergies of the Floquet operator and compare them with the predictions of RMT. The results are presented in Fig. 7 where our numerical results are shown together with the universal (no fit parameters) curves predicted by the random matrix theory.

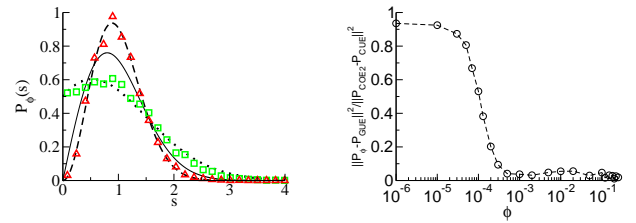


Figure 7: Left panel. Probability distribution for the quasienergies level spacing at $\phi = 0$ (green squares) and at $\phi = \pi/2$ (red triangles). The other curves are obtained from RMT in case of COE (full line), “2-folded” COE (dotted line) and CUE (dashed line). Right panel. $\|P_\phi(s) - P_{CUE}(s)\|^2 / \|P_{COE2}(s) - P_{CUE}(s)\|^2$ as a function of ϕ . $\|\cdot\|$ is the \mathcal{L}^2 norm we use to characterize the distance between curves. $P_{COE2}(s)$ and $P_{CUE}(s)$ are the probability distribution of level spacing obtained from RMT for “2-folded” COE and CUE respectively. P_ϕ is the probability distribution function obtained numerically at different values of ϕ . For both panel $k = 200$ and $K = 10$.

The plots have been obtained by considering a Floquet operator of 2^{10} levels averaged over 10 realizations corresponding to random values of $(\phi_L + \phi_R)/2$ distributed in $[0, 2\pi)$.

For $\phi = 0$ the probability distribution function is in perfect agreement with that of a folded spectrum³⁸. This corresponds to the fact that, at $\phi = 0$, the Floquet operator of our system is $U(T, 0) = F_1 \cdot F_2$, where F_1, F_2 are statistically independent Floquet operators of the usual QKR. The analysis of the transition between the two ensembles is presented in Fig. 7, right panel. We have analyzed the crossover between the two ensembles by looking at the distance, at a generic ϕ , between the distribution P_ϕ and the distribution corresponding to the Circular Unitary Ensemble, P_{CUE} . The distance between the distributions is define by the L^2 norm:

$$\|f(s) - g(s)\| = \left[\int_{\mathbb{R}} (f(s) - g(s))^2 ds \right]^{1/2}.$$

The results are plotted in Fig. 7, right panel. At $\phi = 0$ the distribution coincides with that of a “2-folded” Circular Orthogonal Ensemble. At $\phi \sim 10^{-3}$ the distribution stabilizes to that of a CUE. The crossover between the two ensembles is occurs at $\phi \sim 1/\sqrt{D} = \sqrt{2}/k \sim 5 \cdot 10^{-3}$.

C. Transport properties in the chaotic regime

Up to now we have discussed the chaotic dynamics by looking at the fluctuations of the charge on the central island. The possibility to observe the various fundamental aspects of quantum and classical chaotic behavior in the Cooper pair shuttle has been discussed in Ref. 13. We proceed further in this direction by investigating how the chaotic dynamics affects the transport properties of the

Cooper pair shuttle. The most convenient way to achieve our purpose is provided by the determination of the Full Counting Statistics (FCS) which was already analyzed in the normal shuttle by Pistoiesi³⁹ and in the charge regime

of the Cooper pair shuttle by Romito and Nazarov¹². The generating function of the current cumulants at left and right contacts, defined through

$$\partial_\lambda^n \mathfrak{Z}(\Lambda, \lambda, \tau) |_{\lambda, \Lambda=0} = \frac{(-i)^n}{e^n} \int_{[0, \tau]^{\times n}} dt_1 \cdots dt_n \langle \hat{I}(t_1) \cdots \hat{I}(t_n) \rangle \quad (55)$$

is expressed in terms of the Hamiltonian of the Cooper pair shuttle H_0 in Eq. (47) by

$$\mathfrak{Z}(\lambda_L, \lambda_R, \tau) = e^{-\mathfrak{S}(\lambda_L, \lambda_R, \tau)} = \text{Tr} \left[\underbrace{\hat{\mathcal{U}}_{+\lambda_L, +\lambda_R}(\tau, 0) \rho(0) \hat{\mathcal{U}}_{-\lambda_L, -\lambda_R}^\dagger(\tau, 0)}_{\hat{\rho}^{(\lambda_L, \lambda_R)}(\tau)} \right], \quad (56)$$

$$\hat{\mathcal{U}}_{\lambda_L, \lambda_R}(\tau, 0) = \overrightarrow{T} \exp^{-i \int_0^\tau \hat{H}_{\lambda_L/2, \lambda_R/2}(s) \frac{ds}{\hbar}}, \quad \hat{H}_{\lambda_L/2, \lambda_R/2} = \hat{H}_0(\phi_L \rightarrow \phi_L - \lambda_L, \phi_R \rightarrow \phi_R - \lambda_R). \quad (57)$$

The necessary steps to calculate the FCS are summarized in Appendix C. According to Eq. (57), the task is to calculate the time evolution for $\rho^{(\lambda_L, \lambda_R)}$ which is a modified density matrix in which bra and ket evolves according

to two different Hamiltonians. To this aim we generalize the diagrammatic approach presented in Ref. 40. In the basis of charge eigenstates we write

$$\rho_{n_+, n_-}^{(\lambda_L, \lambda_R)}(t) = \sum_{n'_+, n'_-} G_{n_+, n'_+; n_-, n'_-}^{(\lambda_L, \lambda_R)}(t) \rho_{n'_+, n'_-}(0), \quad (58)$$

$$G_{n_+, n'_+; n_-, n'_-}^{\lambda_L, \lambda_R}(t) = \langle n_+ | \hat{V} \hat{U}_{+\lambda_L, +\lambda_R}^t | n'_+ \rangle \langle n'_- | \hat{U}_{-\lambda_L, -\lambda_R}^{\dagger t} \hat{V}^\dagger | n_- \rangle; \quad (59)$$

t is the time counted in integers multiples of the period T and U_{λ_L, λ_R} is given in Eq. (48) after the replacing $\phi_L \rightarrow \phi_L - \lambda_L$, $\phi_R \rightarrow \phi_R - \lambda_R$. In Eq. (59) we have also added an operator for the free evolution after the last kick for computational convenience; it does not affect the physics because it simply means that we look at all observables just before a kick, rather than just after it. We now turn to the Wigner representation for the kernel G ,

$$\tilde{G}_{n, \Theta; n', \Theta'}^{(\lambda_L, \lambda_R)}(t) = \sum_{n_+ - n_-} \sum_{n'_+ - n'_-} G_{n_+, n'_+; n_-, n'_-}^{(\lambda_L, \lambda_R)}(t) e^{i\Theta(n_+ - n_-)} e^{i\Theta'(n'_+ - n'_-)}, \quad (60)$$

where $n = (n_+ + n_-)/2$ and $n' = (n'_+ + n'_-)/2$ are the “center of mass” coordinates. We compare the kernel in Wigner representation with the classical equivalent kernel for the evolution of a distribution function in the phase space. The classical dynamics is unstable in the Θ direction²³, and therefore we approximate the quantum kernel \tilde{G} by its average over Θ, Θ' . As a consequence the inverse Fourier transform of Eq. (60) picks up non-vanishing terms only at $n_+ = n_-$ and $n'_+ = n'_-$. In doing so, we have reduced Eq. (58) to an evolution equation for the populations of the modified density matrix,

$$\rho_{n, n}^{(\lambda_L, \lambda_R)}(t) = \sum_{n'} G^{(\lambda_L, \lambda_R)}(n, n'; t) \rho_{n', n'}^{(\lambda_L, \lambda_R)}(0), \quad (61)$$

$$G^{(\lambda_L, \lambda_R)}(n, n'; t) = \langle n | \hat{V} \hat{U}_{+\lambda_L, +\lambda_R}^t | n' \rangle \langle n' | \hat{U}_{-\lambda_L, -\lambda_R}^{\dagger t} \hat{V}^\dagger | n \rangle, \quad (62)$$

and therefore

$$\begin{aligned} \mathfrak{Z}(\lambda_L, \lambda_R, t) &= \text{Tr} \{ \rho^{(\lambda_L, \lambda_R)}(t) \} \\ &= \sum_{n, n'} G^{(\lambda_L, \lambda_R)}(n, n'; t) \rho_{n', n'}(0), \end{aligned} \quad (63)$$

We expect that $G^{(\lambda_L, \lambda_R)}(n, n'; t)$ depends only on the difference $n - n'$, and we then average out $(n + n')/2$ as

follows

$$\overline{G}^{(\lambda_L, \lambda_R)}(n - n'; t) \equiv \lim_{L_0 \rightarrow \infty} \sum_{l=-L_0}^{L_0} \frac{G^{(\lambda_L, \lambda_R)}(n + l, n' + l; t)}{2L_0 + 1}. \quad (64)$$

The key observation to construct the perturbation theory is that the average of the kernel can be reabsorbed in an average over the free evolution operators by means of the relation

$$\langle n + l | \hat{V} | n' + l \rangle = \langle n | \hat{W} | n' \rangle, \quad (65)$$

with

$$\langle n | \hat{W} | n' \rangle = \exp[-i\tilde{\kappa}(n - l)^2/2] \delta_{n, n'} \equiv W(n) \delta_{n, n'}. \quad (66)$$

The kernel $G^{(\lambda_L, \lambda_R)}(n - n'; t)$ involves products with an equal number of \hat{W} and \hat{W}^\dagger , therefore the average is completely defined by

$$\begin{aligned} & \overline{W(n_1)W(n_2) \dots W(n_i)W(n'_1)^*W(n'_2)^* \dots W(n'_i)^*} = \\ & = \exp\left[-(i\tilde{\kappa}/2) \sum_a (n_a^2 - n_a'^2)\right] \delta_{\sum_a (n_a - n_a', 0)}. \end{aligned} \quad (67)$$

The potential \hat{W} of the kicked rotator is not Gaussian distributed. However, in the diagrammatic expansion we are going to perform, we will restrict only to two point correlators. Therefore the r.h.s. of Eq. (67) reduces to $\delta_{n, n'}$ and the effects of having a non-Gaussian distribution don't appear⁴⁰. Once the kernel $G^{(\lambda_L, \lambda_R)}(n, n'; t)$ in Eq. (63) has been replaced by the averaged one which depends only on the difference $n - n'$, the sum over n' in the same equation can be performed noting that $\sum_{n'} \rho_{n', n'}(0) = \text{Tr} \rho(0) = 1$. We now turn to phase and frequency space by Fourier transforming the kernel $\overline{G}^{(\lambda_L, \lambda_R)}(n - n'; t)$ both in n, n' and in t , obtaining

$$\mathfrak{Z}(\lambda_L, \lambda_R, t) = \lim_{q \rightarrow 0} \int_0^{2\pi} e^{-i\omega T t} \overline{\mathfrak{G}}^{(\lambda_L, \lambda_R)}(q; \omega). \quad (68)$$

The kernel \mathfrak{G} is defined through

$$\overline{\mathfrak{G}}^{(\lambda_L, \lambda_R)}(\theta, \theta', q, q'; \omega, \omega_0) = \overline{\mathfrak{G}}^{(\lambda_L, \lambda_R)}(q; \omega) \delta(q - q'). \quad (69)$$

with

$$\overline{\mathfrak{G}}^{(\lambda_L, \lambda_R)}(\theta, \theta', q, q'; \omega, \omega_0) = \overline{\langle \theta_+ | \hat{W} \left(1 - e^{i\omega_+ T} \hat{\mathcal{U}}_{(+\lambda_L, +\lambda_R)}\right)^{-1} | \theta'_+ \rangle \langle \theta'_- | \left(1 - e^{-i\omega_- T} \hat{\mathcal{U}}_{(-\lambda_L, -\lambda_R)}^\dagger\right)^{-1} \hat{W}^\dagger | \theta_- \rangle}, \quad (70)$$

$\theta_\pm = \theta \pm q/2$, $\theta'_\pm = \theta' \pm q'/2$, $\omega_\pm = \omega_0 \pm \omega/2$ and $\hat{\mathcal{U}}_{\lambda_L, \lambda_R} = \hat{J}_R \hat{W} \hat{J}_L \hat{W}$. The dependence of $\hat{\mathcal{U}}_{(\lambda_L, \lambda_R)}$ on $\lambda_{L(R)}$ is through $\hat{J}_{L,R} = e^{-ik \cos(\hat{\varphi} - (\phi_{L,R} + \lambda_{L,R}))}$, $\hat{J}_{L,R}^\dagger = e^{ik \cos(\hat{\varphi} - (\phi_{L,R} - \lambda_{L,R}))}$. The diagrammatic perturbation theory consists in a series expansion of the r.h.s. of Eq. (70) in $\hat{J}_R \hat{W} \hat{J}_L \hat{W}$. Any term of the expansion correspond to a diagram which consists of propagators,

$$\begin{aligned} & \begin{array}{c} \xrightarrow{\hat{J}_b} \\ \theta_+ \\ \xleftarrow{\hat{J}_b^\dagger} \\ \theta_- \end{array} = e^{i\omega T} e^{-ik \cos(\theta + \frac{q}{2} - \phi_b - \lambda_b)} e^{ik \cos(\theta - \frac{q}{2} - \phi_b + \lambda_b)}. \end{aligned} \quad (71)$$

and averaged vertices

$$\begin{array}{c} \hat{W} \\ \times \\ \theta_+ \leftarrow \times \rightarrow \theta'_+ \\ \vdots \\ \theta_- \leftarrow \times \rightarrow \theta'_- \\ \times \\ \hat{W}^\dagger \end{array} = \delta(\theta'_+ - \theta_+ - (\theta'_- - \theta_-)). \quad (72)$$

We have absorbed the frequency dependence in the expression for the propagator, from which it is evident that the final expression for the kernel is independent on ω_0 . The average process is indicated by a dotted line in the diagrammatic expression. In any diagrams, correlations

can take place between any pair of vertices one of which in the upper line and the other in the lower line. Any other term involves expressions of the form $\hat{W}\hat{W}$ or $\hat{W}^\dagger\hat{W}^\dagger$ and vanishes accordingly to Eq. (67).

For $k \gg 1$, diagrams involving crossing correlations lines, are parametric small in $1/k$, *i.e.* in $\tilde{\kappa}$. This allows us to approximate, at lowest order in $\tilde{\kappa}$, which is the classical limit, the kernel with the sum of all ladder diagrams, we will refer to as *diffuson*.

Classical limit

The diffuson is defined through the series of ladder diagrams

$$\begin{array}{c} \theta_+ \leftarrow \boxed{\mathcal{D}} \rightarrow \theta'_+ \\ \theta_- \leftarrow \boxed{\mathcal{D}} \rightarrow \theta'_- \end{array} = \begin{array}{c} \hat{W} \\ \times \\ \theta_+ \leftarrow \times \rightarrow \theta'_+ \\ \vdots \\ \theta_- \leftarrow \times \rightarrow \theta'_- \\ \times \\ \hat{W}^\dagger \end{array} + \begin{array}{c} \hat{W} \quad \hat{J}_R \quad \hat{W} \quad \hat{J}_L \quad \hat{W} \\ \times \quad \times \quad \times \quad \times \quad \times \\ \theta_+ \leftarrow \times \rightarrow \theta'_+ \\ \vdots \\ \theta_- \leftarrow \times \rightarrow \theta'_- \\ \times \quad \times \quad \times \quad \times \quad \times \\ \hat{W}^\dagger \quad \hat{J}_R^\dagger \quad \hat{W}^\dagger \quad \hat{J}_L^\dagger \quad \hat{W}^\dagger \end{array} + \dots \quad (73)$$

The computation of the diffuson become simple due to Eq. (72). It allows to factorize any diagram as products of

$$\zeta(q; \omega) = \frac{\begin{array}{c} \xrightarrow{\hat{W}} \xrightarrow{\hat{J}_R} \times \xrightarrow{\hat{W}} \xrightarrow{\hat{J}_L} \times \xrightarrow{\hat{W}} \\ \theta_{1+} \quad \theta_{2+} \\ \xleftarrow{\hat{W}^\dagger} \xleftarrow{\hat{J}_R^\dagger} \times \xleftarrow{\hat{W}^\dagger} \xleftarrow{\hat{J}_L^\dagger} \times \xleftarrow{\hat{W}^\dagger} \\ \theta_{1-} \quad \theta_{2-} \end{array}}{1} = J_0(2k \sin(q/2 - \lambda_L)) J_0(2k \sin(q/2 - \lambda_R)) e^{i\omega T} . \quad (74)$$

then the series is a geometric series and we find

$$\mathcal{D}^{(\lambda_L, \lambda_R)}(q, q'; \omega) = \delta(q - q') \sum_{i=0}^{\infty} [\zeta(q; \omega)]^i = \frac{1}{1 - e^{i\omega T} J_0(2k \sin(q/2 - \lambda_L)) J_0(2k \sin(q/2 - \lambda_R))} \delta(q - q') . \quad (75)$$

By replacing $\overline{\mathfrak{G}}^{(\lambda_L, \lambda_R)}(q, \omega)$ with $\mathcal{D}^{(\lambda_L, \lambda_R)}(q, q'; \omega)$ in Eq. (68), we finally find

$$\mathfrak{Z}(\lambda_L, \lambda_R, t) = e^{-\mathfrak{G}(\lambda_L, \lambda_R)t} = [J_0(2k \sin \lambda_L) J_0(2k \sin \lambda_R)]^t . \quad (76)$$

It defines all transport properties of the system. In particular the probability of charge transfer per cycle at a given contact is

$$\begin{aligned} p_N^{L(R)} &= \lim_{\lambda_R, \lambda_L \rightarrow 0} \frac{1}{2\pi} \int_0^{2\pi} d\lambda_{L(R)} e^{\mathfrak{G}(\lambda_L, \lambda_R)} e^{-i\lambda_{L(R)} N} \\ &= \sum_{M \in \mathbb{Z}} \delta_{N, 2M} J_M^2(k) . \end{aligned} \quad (77)$$

The properties of Bessel functions guarantees the normalization condition $\sum_N p_N = 1$. Probabilities are non-vanishing only for even numbers of electrons, i.e. Cooper pairs. Note also that the very same existence of such probabilities means that the transport is completely incoherent and the chaotic dynamics is efficient in destroying any features of the coherent superconducting nature of the transfer.

The low frequency noise at various contact is easily determined

$$S_L(\omega = 0) = S_R(\omega = 0) = k^2/4 , \quad (78)$$

while the correlations between left and right currents is vanishing:

$$\int_{\mathbb{R}} \langle I_L(0) I_R(t) \rangle = 0 . \quad (79)$$

The limit $\lambda_{L,R} \rightarrow 0$ of Eq. (75) gives us the kernel for the evolution of the density matrix in the classical limit. In particular, for long time and large $n - n'$ ($\omega \rightarrow 0$, $q \rightarrow 0$),

$$\mathcal{D}(q, q'; \omega) \approx \frac{1}{(kq)^2/2 - i\omega T t} \delta(q - q') . \quad (80)$$

which expresses the diffusive behavior in $n - n'$ with diffusion constant $D = k^2/2$ in complete agreement with the

results obtained from the classical map. It correctly reproduces the result obtained in Ref. 40. The dependence on ϕ disappears from the final expression. In fact we do not recover the classical effects in Eq. (53) because we just restrict our considerations to single impurity correlations, while the dependence on ϕ comes from higher time correlations (see Appendix B). It is possible to reproduce the classical corrections to the diffusion constant within the diagrammatic approach. This has been performed in Ref. 41 for $\phi = 0$.

Beyond the classical limit

All the diagrams not included in the diffuson contain crossing between two vertex correlation lines. They should therefore be parametric small in $1/k$. There is, however, a special crossing diagram which contributes at the same order of the diffuson. It is the cooperon:

$$\begin{array}{c} \theta_+ \quad \theta'_+ \\ \theta_- \quad \theta'_- \end{array} \boxed{\mathcal{C}} = \begin{array}{c} \xrightarrow{\hat{W}} \times \xrightarrow{\hat{J}_R} \times \xrightarrow{\hat{W}} \times \xrightarrow{\hat{J}_L} \times \xrightarrow{\hat{W}} \\ \theta_{1+} \quad \theta_{2+} \quad \theta_{2+} \quad \theta_{1+} \\ \xleftarrow{\hat{W}^\dagger} \times \xleftarrow{\hat{J}_R^\dagger} \times \xleftarrow{\hat{W}^\dagger} \times \xleftarrow{\hat{J}_L^\dagger} \times \xleftarrow{\hat{W}^\dagger} \\ \theta_{1-} \quad \theta_{2-} \quad \theta_{2-} \quad \theta_{1-} \end{array} + \dots \quad (81)$$

The cooperon diagram is topologically equivalent to a diffuson diagram after time reversion of the lower line,

$$\begin{array}{c} \theta_+ \quad \theta'_+ \\ \theta_- \quad \theta'_- \end{array} \boxed{\mathcal{C}} = \begin{array}{c} \xrightarrow{\hat{W}} \times \xrightarrow{\hat{J}_R} \times \xrightarrow{\hat{W}} \times \xrightarrow{\hat{J}_L} \times \xrightarrow{\hat{W}} \\ \theta_{1+} \quad \theta_{2+} \quad \theta_{2+} \quad \theta_{1+} \\ \xleftarrow{\hat{W}^\dagger} \times \xleftarrow{\hat{J}_R^\dagger} \times \xleftarrow{\hat{W}^\dagger} \times \xleftarrow{\hat{J}_L^\dagger} \times \xleftarrow{\hat{W}^\dagger} \\ \theta_{1-} \quad \theta_{2-} \quad \theta_{2-} \quad \theta_{1-} \end{array} + \dots \quad (82)$$

In this form the correlation lines do not cross and it is therefore clear that the contribution of the cooperon series

is at same order of the diffuson's one. The form of the cooperon in Eq. (82) leads to

$$\mathcal{C}(\vartheta, \vartheta'; \omega) = \frac{1}{1 - e^{i\omega T} J_0(2k \sin(\vartheta/2 - (\lambda_L/2 - \lambda_R/2))) J_0(2k \sin(\vartheta'/2 + \phi - (\lambda_R/2 - \lambda_L/2)))} \delta(\vartheta - \vartheta'), \quad (83)$$

with $\vartheta = \theta_+ + \theta'_-$, $\vartheta' = \theta'_+ + \theta_-$. At $\lambda_L = \lambda_R = 0$ our equations describe the time evolution of the density matrix of the system. In this case the low frequency small angle limit is affected by ϕ as well,

$$\mathcal{C}(\vartheta, \vartheta'; \omega) \approx \frac{1}{k^2/4 [\vartheta^2 + (\vartheta + 2\phi)^2] - i\omega T t} \delta(\vartheta - \vartheta'). \quad (84)$$

By Fourier transforming the previous equation with respect to time and phase it can be easily seen that the diffusive behavior is modified by the presence of ϕ introducing a relaxation time $\tau_\phi = [(k\phi)^2/2]$. At $\tau_\phi \sim 1$, which is $\phi \sim 1/\sqrt{D}$, the cooperon contribution is completely suppressed.

The calculation of quantum corrections to the classical diffuson in the diagrammatic approach is based on writing a Dyson equation for the four point vertex $\overline{\mathcal{G}}^{(\lambda_L=0, \lambda_R=0)}(\theta, \theta', q, q'; \omega, \omega_0)$, as discussed by Altland⁴⁰. In this procedure, due to probability conservation, the leading quantum corrections are determined only by the most infrared divergent terms of the diagrammatic expansion. At $\phi = 0$ the most infrared divergent term is given by the cooperon and quantum correction can be computed, while this is not the case at $\phi \neq 0$ (form Eq. (84), $\lim_{\omega \rightarrow 0, \theta \rightarrow 0} \mathcal{C}(\vartheta, \vartheta'; \omega)$ is finite) where, due to the breaking of time reversal symmetry, the diagrammatic approach does not work⁴⁰.

We did not succeed in extending the diagrammatic approach to compute the quantum corrections to the full counting statistics. Even in the case of $\phi = 0$ quantum corrections to the classical result for the FCS cannot be determined by the perturbation theory. In fact the possibility of writing a Dyson equation for the vertex function crucially relies on the existence of a Ward identity corresponding to probability conservation⁴⁰, $\text{Tr}\{\rho(t)\} = 1$. Due to presence of the counting fields in the kernel $G^{(\lambda_L, \lambda_R)}(n, n'; t)$, $\text{Tr}\{\rho^{(\lambda_L, \lambda_R)}\} \neq 1$, and a similar conservation law cannot be established when the counting fields are inserted in the propagators.

Anyway the perturbative calculations of quantum corrections cannot give us quantitative information on the quantum steady state of the system⁴⁰, i.e. the dynamical localized state. In this regime we can easily estimate the average value of the current and the fluctuations of the current signal. This is achieved assuming random uncorrelated phases for the localized wave function of the grain:

$$|\psi\rangle = \frac{1}{\sqrt{2l+1}} \sum_{n=-l}^l e^{i\alpha_n} |n\rangle, \quad (85)$$

$$P(\alpha_n) = 1/(2\pi) \quad \alpha_n \in [0, 2\pi). \quad (86)$$

It follows that

$$\overline{I_{L(R)}} = 0, \quad (87)$$

$$\sqrt{\overline{I_{L(R)}^2}} = \frac{2e}{T\sqrt{2l+1}}, \quad (88)$$

where the $\overline{}$ defines (only in Eq. (87, 88)) the average over the random phases of the usual Josephson current $\hat{I}_{L(R)} = 2e\frac{k}{T} \langle \sin(\hat{\varphi} - \phi_{L(R)}) \rangle$ defined in Eq. (5, 6).

V. CONCLUSIONS

The Cooper pair shuttle is a very rich system where to study various aspects of coherence quantum dynamics of driven systems. In this work we concentrated on two different regimes where the charging energy is either much smaller or much larger than the Josephson coupling energy. In both cases we analyzed the transport properties as the Josephson current or the current fluctuations. In the charge regime we evaluated both the DC and AC Josephson effect. In the other regime we analyzed the consequences of the underlying classical chaotic dynamics on the full counting statistics.

We believe that the possibility to realize periodic driving via time-dependent fluxes opens the possibility to study the very exciting area of quantum driven systems in variety of different situations beyond that considered in this paper.

Acknowledgments

We acknowledge useful discussions with F. Plastina, G. Benenti, A. Kamenev, and Yu. V. Nazarov. This work was supported by EC through grant EUROSQIP and by MIUR through PRIN.

Appendix A: EFFECT OF NON-DEGENERACY DURING THE CYCLE

In this Appendix we discuss the Josephson current in the Cooper pair shuttle when the gate voltage fluctuates around a fixed value away from the degeneracy point even during the connection to the electrodes. In Section III we assumed $n_g(t) = 1/2$ during the Josephson contacts to enhance the Cooper pair transfer and $n_g(t) = \text{const.} \neq 0$ during the free evolution time. From an experimental point of view, however, it would be easier to avoid this periodical modification of the gate voltage V_g . It can be

therefore interesting to have an expression for the DC Josephson current in the case of constant gate voltage.

If $n_g(t) = \text{const.} = 1/2$, the Josephson current can be obtained from the expressions of section III with the replacement $\chi_{\rightarrow} = \chi_{\leftarrow} = 0$. If $n_g(t) = \text{const.} \neq 1/2$, instead, the general expression for the current (Eq. (23)) still holds, but differences arise in the explicit form of matrix M_0 and vector \mathbf{v}_0 . During the free evolution time intervals the dynamics is unchanged compared to the case discussed before. In the L and R regions instead, we have to include in the Hamiltonian the term proportional to the charging energy difference, E_C , between the two charge states. The Hamiltonian (system and bath), in the basis which diagonalizes the Cooper pair box Hamiltonian now reads

$$H = \frac{E}{2}\sigma_z + \hat{O}(\cos(2\mu)\sigma_z + \sin(2\mu)\sigma_x) + H_{\text{bath}}, \quad (\text{A1})$$

where \mathcal{O} is the same of Eq. (10), and

$$E = (E_C^2 + E_J^2)^{1/2}, \quad \cos(2\mu) = E_C/E.$$

The Hamiltonian in Eq. (A1) has been widely studied¹⁸. In Born-Markov and Rotating Wave approximations the time evolution of populations (diagonal terms) in the reduced density matrix and coherences (off-diagonal ones) are still independent. The respective decoherence rates

read

$$\gamma_J^{\text{pop.}} = 2\gamma_J \sin^2(2\mu), \quad (\text{A2})$$

$$\gamma_J^{\text{coher.}} = \gamma_J \sin^2(2\mu) + \Gamma_J \cos(2\mu). \quad (\text{A3})$$

We notice that we have to introduce two different dephasing rates, γ_J and Γ_J . In our approximation, they are $\gamma_J = (\pi/2)\alpha E \coth(E/T_b)$, and $\Gamma_J = 2\pi\alpha T_b$, in case of weak coupling of the system to the bath ($\alpha \ll 1$). Depending on the relative strength of the two energy scales E_C and E_J , we have different effects. If $E_C = 0$, (corresponding to $2\mu = \pi/2$) we recover the Hamiltonian of the early case described in section III. If $E_C \ll E_J$, we have corrections of order E_C/E_J in our previous results, and we are not interested in them as we get a finite result at zero order in E_C/E_J . In the opposite limit $E_J \ll E_C$, the situation is quite different. If one neglects E_J , the current vanishes because \hat{n} is a constant of motion. The first non vanishing term must be of order E_J/E_C . Below we give the analytical expression for the current in the limit of strong dephasing (for $t_L = t_R = t_J$ and $t_{\rightarrow} = t_{\leftarrow} = t_C$) including only the leading order in E_J/E_C . The strong dephasing limit refers to the condition $\gamma_J t_J, \Gamma_J t_J, \gamma_C t_C \gg 1$, which allows a series expansion of the Josephson current at first order in $e^{-\gamma_J t_J}$, $e^{-\Gamma_J t_J}$ and $e^{-\gamma_C t_C}$:

$$I_{\text{strong}} \sim -\frac{2e}{T} \tanh\left(\frac{E_C}{T_b}\right) \left(\frac{E_J}{E_C}\right)^2 \sin\phi e^{-\gamma_C t_C} \left[\sin(2\chi) \left(\cos(2\theta) e^{-\gamma^{\text{coher.}} t_J} - e^{-\gamma^{\text{pop.}} t_J} \right) + \cos(2\chi) e^{-\gamma^{\text{coher.}} t_J} \right]. \quad (\text{A4})$$

In this case the Josephson energy does not any more enter the current through the combination $E_J t_J$ as in the previous case, but rather it appears through the ratio E_J/E_C . There is an overall suppression factor $\propto (E_J/E_C)^2$. Note that the dependence on the dynamical phase χ is not the same of that in Eq. (29). The ap-

proximation $E_J \ll E_C$ also induces a hierarchy in the dephasing rates, $\gamma_J^{\text{coher.}} \gg \gamma_J^{\text{pop.}} \sim 2(E_J/E_C)^2 \gamma_J$. Within such approximation, we can neglect terms of order $e^{-\Gamma_J t_J}$ with respect to 1 (or equivalently $e^{-\gamma^{\text{coher.}} t_J}$ with respect to $e^{-\gamma^{\text{pop.}} t_J}$) in the current expression, leading to

$$I_{\text{strong}} \sim -\frac{2e}{T} \tanh\left(\frac{E_C}{T_b}\right) \left(\frac{E_J}{E_C}\right)^2 e^{-\left(2\left(\frac{E_J}{E_C}\right)^2 \gamma_J t_J + \gamma_C t_C\right)} \sin(2\chi) \sin\phi. \quad (\text{A5})$$

The exponential suppression due to dephasing in the Josephson contact times is reduced by the factor $\sin(2\mu) \sim (E_J/E_C)^2$.

Appendix B: PHASE DEPENDENT CORRECTIONS TO THE CLASSICAL DIFFUSION

In this Appendix we derive Eq. (53) for the charge diffusion coefficient obtained for the modified Chirikov map in Eq. (52). The starting point of the calculation,

following the idea of Ref. 32, is to rewrite the Eq. (52),

$$\begin{cases} p_t = p_{t-1} - K \sin \{ \theta_{t-1} - [(t+1) \bmod 2] \phi \} \\ \theta_t = \theta_{t-1} + p_t, \end{cases} \quad (\text{B1})$$

$$P(\theta, n; t) = \int_0^{2\pi} G(\theta - \theta', n) P(\theta', n + K \sin \{ \theta' - [(t+1) \bmod 2] \phi \}; t-1) dx, \quad (\text{B2})$$

where t counts the number of kicks. The kernel G defines the random step between two kicks,

$$G(\delta\theta, n) = \frac{1}{\sqrt{2\pi}\sigma} \sum_{m=-\infty}^{+\infty} \exp \left[-\frac{(\delta\theta - n + 2\pi m)^2}{2\sigma} \right] = \frac{1}{2\pi} \sum_{m=-\infty}^{\infty} e^{-\sigma m^2/2} e^{im(\delta\theta - n)}. \quad (\text{B3})$$

It correspond to add a diffusive term ($\sigma/2$ the diffusion coefficient) in the differential equation for the time evolution between two kicks. In this way we have replaced the deterministic dynamics of Eq. (B1) with a stochastic one which reproduce the effect of chaotic dynamics. At the end of the calculations we can take the limit $\sigma \rightarrow 0$.

By introducing the Fourier coefficients for the probability distribution function $P(\theta, n; t)$ defined through

$$P(\theta, n; t) = \frac{1}{(2\pi)^2} \sum_{m=-\infty}^{\infty} \int_{\mathbb{R}} dp a_m^{(t)}(p) e^{i(m\theta + pn)}, \quad (\text{B4})$$

we can write the diffusion coefficient as

$$D = \frac{1}{2t} \langle n^2 \rangle = \frac{1}{2t} \lim_{p \rightarrow 0^+} \left(i \frac{\partial}{\partial p} \right)^2 a_0^{(t)}(p). \quad (\text{B5})$$

We have implicitly assumed that $p_0 = 0$. We now rewrite the time evolution in Eq. (B2) in the Fourier space and then we expand in powers of $1/\sqrt{K}$. The first step is performed by simply inserting Eq. (B3, B4) into Eq. (B2). After some algebra, we find

$$a_m^{(2t)}(p) = \left[\sum_{l=-\infty}^{+\infty} J_l(K|p'|) e^{i\phi \operatorname{sgn}(p')} e^{-\sigma m^2/2} \right] a_{m'}^{(2t-1)}(p') \quad (\text{B6})$$

$$a_m^{(2t+1)}(p) = \left[\sum_{l=-\infty}^{+\infty} J_l(K|p'|) e^{-\sigma m^2/2} \right] a_{m'}^{(2t)}(p') \quad (\text{B7})$$

$$p' = p + m \quad m' = m - l \operatorname{sgn}(p'), \quad (\text{B8})$$

where $J_l(x)$ is the l th Bessel function.

If we represent the variables p and m respectively in the x -axis and y -axis in the plane, Eq. (B8) defines a path in such a plane. The calculations of the diffusion constant through Eq. (B5) is therefore reduced to the calculation of $a_m^{(t)}(p)$ along the path defined by Eq. (B8). Indeed many path can contribute and one has to sum over them. As it is evident from Eq. (B5) only terms of $a_m^{(t)}(p)$

as a time evolution equation for the probability distribution function in the phase space, $P(\theta, n; t)$ in which we add a further random step. It reads

linear in time are important, therefore we can consider an even number of periods. We assume the initial condition $a_m^{(t=0)}(p) = \delta_{m,0} \delta_{p,0^+}$. Then, from Eq. (B8) the first step of the path is either $(0, 0) \rightarrow (-1, 1)$, or $(0, 0) \rightarrow (1, -1)$, or $(0, 0) \rightarrow (0, 0)$. From Eq. (B5) we realize that also the final point of the path have to be at $m = 0$. The number of steps of the path correspond to the number of kicks. A trivial path consists in remaining at the origin,

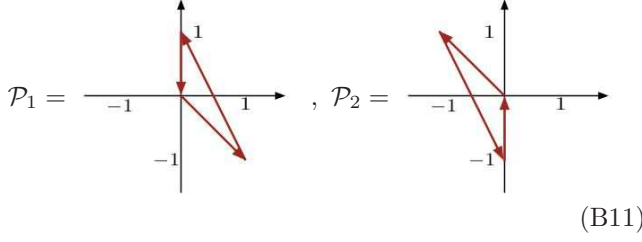
$$\underbrace{(0^+, 0) \rightarrow (0^+, 0) \rightarrow \dots \rightarrow (0^+, 0)}_{2t+1}. \quad (\text{B9})$$

The contribution of this path is

$$a_0^{(2t)}(p \rightarrow 0^+) = [J_0(K|p|)]^{2t} a_0^{(0)}(p) \approx \left[1 - 2t \left(\frac{Kp}{2} \right)^2 \right] a_0^{(0)}(0), \quad (\text{B10})$$

which, combined with Eq. (B5), gives $D = K^2/4$. This is the standard result corresponding to the zero order term in $1/\sqrt{K}$ expansion. Any other term corresponds to a path with steps moving away from the origin. Any such step in the maps in Eq. (B6, B7) involves a Bessel function $J(x \sim K)$, which, in the limit $K \gg 1$ decays like $\sim 1/\sqrt{K}$. Therefore a perturbation in $1/K$ is a perturbation in the number of steps away from the origin in the path. The path in Eq. (B9) is the only contribution at zero order and it is independent on the phase difference ϕ .

The first correction to the result in Eq. (B10) involves the path $(0, 0) \rightarrow (1, -1) \rightarrow (0, 1) \rightarrow (0, 0)$ and its symmetric with respect to the origin of axes. By identifying the path with its numerical value, we write the corrections to the diffusion constant as $\delta D = \mathcal{P}_1 + \mathcal{P}_2$, with



(B11)

$$\begin{aligned}
 a_0^{(2t)}(p \rightarrow 0^+) &= (2t-2) [J_0(Kp)]^{2t-3} J_{-1}(Kp) e^{-i\phi} J_2((p+1)K) e^{-\sigma/2} J_{-1}(Kp) e^{-i\phi} e^{-\sigma/2} a_0^{(0)}(p) \\
 &\approx (2t-2) \left(\frac{Kp}{2}\right)^2 e^{-2i\phi-\sigma} J_2(K).
 \end{aligned} \tag{B12}$$

The same procedure leads to $\mathcal{P}_2 = \mathcal{P}_1(\phi \rightarrow -\phi)$. We can now determine the correction to the diffusion coefficient:

$$D = \frac{K^2}{4} [1 - 2 \cos(2\phi) J_2(K)] + \mathcal{O}\left(\frac{1}{K}\right), \tag{B13}$$

If we observe that we measured time in number of kicks, *i.e.* in units of $T/2$, Eq. (B13) exactly coincides with Eq. (53), in which time is measured in units of T .

Appendix C: FULL COUNTING STATISTICS OF COOPER PAIR SHUTTLING

In this appendix we briefly review the technique of Full Counting Statistics (FCS) introduced in the seminal paper of Levitov and Lesovik⁴² and developed by Nazarov *et al.* (see Ref. 43). We use such formalism to obtain Eq. (56, 57) presented in the text.

Consider a conductor in which the charge dynamics is determined by the Hamiltonian \hat{H}_{sys} . We are interested in the statistics of the current operator \hat{I} through a given Section of the conductor.

We introduce the function $\mathfrak{Z}(\Lambda, \lambda, \tau) = \exp[-\mathfrak{S}(\Lambda, \lambda, \tau)]$, we will refer to as full counting statistics, formally defined through

$$\mathfrak{Z}(\Lambda, \lambda, \tau) = \text{Tr} \left[\underbrace{\hat{\mathcal{U}}_{+\lambda}(\tau, 0) \rho(\hat{0}) \hat{\mathcal{U}}_{-\lambda}^\dagger(\tau, 0)}_{\hat{\rho}^{(\lambda)}(\tau)} \right], \tag{C1}$$

$$\hat{\mathcal{U}}_{\pm\lambda}(\tau, 0) = \overrightarrow{T} \exp^{-i \int_0^\tau \hat{H}_{\Lambda \pm \lambda/2}(s) \frac{ds}{\hbar}} \tag{C2}$$

$$\hat{H}_{\Lambda \pm \lambda/2} = \hat{H}_{\text{sys}} - \frac{\hbar}{e} (\Lambda \pm \lambda/2) \hat{I}. \tag{C3}$$

In this expression the density matrix of the system is let evolve in time according to two different Hamiltonians for

In calculating the contribution of the first of the two paths we have to consider that the steps out of the origin can start at any of the $(2t-2)$ intermediate steps

bra and ket. The trace of this “modified” density matrix is the full counting statistics. The difference between the two Hamiltonians is due to the presence of $\lambda \neq 0$, that is called counting field. It can be seen by direct verification that $\mathfrak{Z}(\Lambda, \lambda, \tau)$ is the generating function of current moments:

$$\partial_\lambda^n \mathfrak{Z}(\Lambda, \lambda, \tau)|_{\lambda, \Lambda=0} = \frac{(-i)^n}{e^n} \int_{[0, \tau] \times_n} dt_1 \dots dt_n \langle \hat{I}(t_1) \dots \hat{I}(t_n) \rangle. \tag{C4}$$

Let us also observe that the derivative of $\mathfrak{S}(\Lambda, \lambda, \tau)$ gives us the cumulants of the current instead of its moments:

$$\begin{aligned} \partial_\lambda^n \mathfrak{S}(\Lambda, \lambda, \tau)|_{\lambda, \Lambda=0} &= -\partial_\lambda^n (\ln \mathfrak{Z}(\Lambda, \lambda, \tau))|_{\lambda, \Lambda=0} = \\ &= (-i/e)^n \int_{[0, \tau] \times_n} dt_1 \dots dt_n \langle \hat{I}(t_1) \dots \hat{I}(t_n) \rangle_{\text{conn.}}, \end{aligned} \tag{C5}$$

where $\langle \cdot \rangle_{\text{conn.}}$ indicates the cumulant of the distribution function. The FCS can be adapted to determine various integrated correlators differing in the time ordering of the current operators and to obtain the correlation functions at arbitrary times rather than the integrated ones, thus revealing as a powerful tools in the investigation of the transport properties of a system.

Since the FCS can provide us information about the transport properties of the system, it would be meaningful to have an interpretation of $\mathfrak{Z}(\Lambda, \lambda, \tau)$ directly in terms of charge transfer. As we are interested in the transport properties of a given system contacted to two electron reservoirs,⁵⁰ the properties of the system are fully characterized by the knowledge of the probability $P_\tau(N)$ of transferring N charges in a given time interval τ . $P_\tau(N)$ is equivalently defined by its generating function $\chi(\lambda) = \sum_N P_\tau(N) \exp(iN\lambda)$. In particular all moments of the current distribution function can be obtained as

$$\int_{[0,\tau]^{\times m}} dt_1 \dots dt_m \langle \hat{I}(t_1) \dots \hat{I}(t_m) \rangle = \sum_N (eN)^m P_\tau(N) = (-ie)^m \partial_\lambda^m \chi(\lambda)|_{\lambda=0}. \quad (\text{C6})$$

Due to the relation between the current moments and the function $\chi(\lambda)$, it would appear natural to interpret the $\mathfrak{Z}(\lambda, \Lambda, \tau)$ just constructed as the generating function of the probabilities $P_\tau(N)$. It can be shown that

$$P_\tau(\Lambda, N) = \frac{1}{2\pi} \int_0^{2\pi} d\lambda \mathfrak{Z}(\Lambda, \lambda, \tau) e^{-iq\lambda} \quad (\text{C7})$$

is a positive defined probability if $\mathfrak{Z}(\lambda, \Lambda, \tau)$, is independent on Λ , in which case also $P_\tau(\Lambda, N)$ is.

Despite the previous analysis there are cases in which an interpretation of the transport properties in terms of classical probabilities is not possible. Coherent charge transfer between superconductors is a paradigmatic example. The interpretation of the FCS in this case has been discussed in literature (see Ref. 44 and references therein). Here we just notice that the appearance of non-positive or imaginary values of $P_\tau(\Lambda, N)$ are signature of the coherent nature of charge transfer between superconductors.

We need to adapt the procedure to the case of a tunnel junction where the current operator is defined in terms of creation and annihilation operator in the two different leads. Due to the linear coupling between the current and the counting field λ in Eq. (C3), charge conservation ensures us that the counting field fulfills all properties of a $U(1)$ gauge field. In other words it means that the counting field plays the same role of the electromagnetic field, \mathbf{A} . In the case of a tunnel junction between two electrons reservoirs we are interested in the current through the region between the two leads. The Hamiltonian is

$$\hat{H} = \sum_{A=L,R} E_k \hat{c}_{A,k}^\dagger \hat{c}_{A,k} + \hat{H}_T + \hat{H}_T^\dagger, \quad (\text{C8})$$

$$\hat{H}_T = \sum_{k,h} T_{k,h} \hat{c}_{R,k}^\dagger \hat{c}_{L,h}, \quad (\text{C9})$$

where E_k is the k -dependent energy of electrons in the reservoirs, $T_{k,h}$ the tunneling amplitudes and $c_{L(R),k}$, $c_{L(R),k}^\dagger$ are respectively the annihilation and creation operator for electrons in the left (right) reservoir. As the Hamiltonian is written in terms of operator defined at spatially separated points -that is at left (L) at right leads (R)-, we have to insert the counting field in the only way compatible with the $U(1)$ symmetry of the theory. It means that the counting field must enter through

the Wilson line⁴⁵,

$$\exp \left(i \int_{L \rightarrow R} \mathbf{A} \cdot d\mathbf{r} \right) = e^{-i(\Lambda + \lambda/2)}. \quad (\text{C10})$$

It results in a λ -dependent Hamiltonian $\hat{H}_{\Lambda + \lambda/2}$ obtained by the Hamiltonian in Eq. (C8) after the replacement

$$\hat{H}_T \rightarrow e^{-i(\Lambda + \lambda/2)} \hat{H}_T. \quad (\text{C11})$$

Indeed the integral in Eq. (C10) depends on the specific path going from the left to the right lead, but, in our case, the parameter $\Lambda \pm \lambda/2$ is defined in terms of the whole integral and, thus, the path-dependence in Eq. (C10) is irrelevant. We can now construct the FCS for the Cooper pair shuttle.

The model system we refer to is defined in Section II. For sake of simplicity, here we consider only the case $t_L = t_R = t_J$, $E_J^{(L)} = E_J^{(R)} = E_J$, and $t_{\rightarrow} = t_{\leftarrow} = t_C$. We consider the counting statistics for electrons passing through a counter at left lead. According to the general procedure just described, we have to construct $\hat{H}_{\Lambda + \lambda/2}$ for a tunneling Hamiltonian. This is achieved in Eq. (C11). In the Hamiltonian of the Cooper pair shuttle, Eq. (47), the tunneling term corresponds to the creation of a Cooper pair (of charge $2e$) into the grain, therefore the modification of the Hamiltonian in Eq (C11) is given by

$$|n+1\rangle \langle n| \longrightarrow e^{-i(2\Lambda + \lambda)} |n+1\rangle \langle n|, \quad (\text{C12})$$

or equivalently

$$\hat{H}_{\Lambda \pm \lambda/2} = \hat{H}_0(\phi_L \rightarrow \phi_L + 2\Lambda \pm \lambda). \quad (\text{C13})$$

In this way λ is counting the charge in units of e . Note that Λ can be reabsorbed into ϕ_L by the redefinition $\phi_L + \Lambda \rightarrow \phi_L$. Therefore, as long as the FCS depends on ϕ , it will depend on Λ and the interpretation in terms of probabilities that a certain number of Cooper pairs have traversed the shuttle will be impossible. The construction of the FCS including counting fields both at left and right contacts is straightforward and gives

$$\hat{H}_{\lambda_L/2, \lambda_R/2} = \hat{H}_0(\phi_L \rightarrow \phi_L - \lambda_L, \phi_R \rightarrow \phi_R - \lambda_R), \quad (\text{C14})$$

as presented in Eq. (57).

¹ J. Bardeen, L. N. Cooper, and R. Shrieffer, Phys. Rev. **108**, 1175 (1957).

² B. D. Josephson, Phys. Lett. **1**, 251 (1962).

- ³ M. Tinkham, *Intoduction to Superconductivity* (Mc Graw-Hill, New York, 1966).
- ⁴ A. Barone and G. Paternó, *Physics and Applications of the Josephson Effect* (Wiley, New York, 1982).
- ⁵ Y. Makhlin, G. Schön, and A. Shnirman, *Rev. Mod. Phys.* **37**, 357 (2001).
- ⁶ H. Grabert and M. H. Devoret, eds., *Single Charge Tunneling*, vol. B294 of *NATO ASI* (Plenum Press, New York, 1992).
- ⁷ R. P. Andres, T. Bein, M. Dorogi, S. Feng, J. I. Henderson, C. Kubiak, W. Mahoney, R. G. Osifchin, and R. Reifenberger, *Science* **272**, 1323 (1996).
- ⁸ R. I. Shekhter, Y. Galperin, L. Y. Gorelik, A. Isacsson, and M. Jonson, *J. Phys.: Condens. Matter* **15**, R441 (2003).
- ⁹ L. Y. Gorelik, A. Isacsson, Y. M. Galperin, R. I. Shekhter, and M. Jonson, *Nature* **411**, 454 (2001).
- ¹⁰ A. Isacsson, L. Y. Gorelik, R. I. Shekhter, Y. M. Galperin, and M. Jonson, *Phys. Rev. Lett.* **89**, 277002 (2002).
- ¹¹ A. Romito, F. Plastina, and R. Fazio, *Phys. Rev. B* **68**, 140502(R) (2003).
- ¹² A. Romito and Y. V. Nazarov, *Phys. Rev. B* **70**, 212509 (2004).
- ¹³ S. Montangero, A. Romito, G. Benenti, and R. Fazio, *Europhys. Lett.* **71**, 893 (2005).
- ¹⁴ A. Erbe, R. H. Blick, A. Tike, A. Kriele, and J. P. Kotthaus, *Appl. Phys. Lett.* **73**, 3751 (1998).
- ¹⁵ A. Erbe, C. Weiss, W. Zwerger, and R. H. Blick, *Phys. Rev. Lett.* **87**, 096106 (2001).
- ¹⁶ Y. Nakamura, Y. A. Pashkin, and J. S. Tsai, *Nature* **398**, 786 (1999).
- ¹⁷ O. Buisson, F. Balestro, J. Pekola, and F. W. J. Hekking, *Phys. Rev. Lett.* **90**, 238304 (2003).
- ¹⁸ U. Weiss, *Quantum Dissipative Systems* (World Scientific, Singapore, 1999).
- ¹⁹ A. V. Shytov, D. A. Ivanov, and M. V. Feigel'man, *cond-mat/0110490*.
- ²⁰ C. Cohen-Tannoudji, J. Dupont-Roc, and G. Grynberg, *Atom-Photon interactions* (Wiley, New York, 1992).
- ²¹ G. M. Palma, K. A. Suominen, and A. K. Ekert, *Proc. Roy. Soc. Lond. A* **452**, 567 (1996).
- ²² J. H. Reina, L. Quiroga, and N. F. Johnson, *Phys. Rev. A* **65**, 032326 (2002).
- ²³ F. M. Izrailev, *Phys. Rep.* **196**, 299 (1990).
- ²⁴ F. L. Moore, J. C. Robinson, C. F. Bharucha, B. Sundaram, and M. G. Raizen, *Phys. Rev. Lett.* **75**, 4598 (1995).
- ²⁵ H. Ammann, R. Gray, I. Shvarchuck, and N. Christensen, *Phys. Rev. Lett.* **80**, 4111 (1998).
- ²⁶ C. Zhang, J. Liu, M. G. Raizen, and Q. Niu, *Phys. Rev. Lett.* **92**, 054101 (2004).
- ²⁷ D. M. Basko and V. E. Kravtsov, *Phys. Rev. Lett.* **93**, 056804 (2004).
- ²⁸ B. J. Klappauf, D. A. Oskay, D. A. Steck, and M. G. Raizen, *Physica D* **131**, 78 (1999).
- ²⁹ G. Casati, B. V. Chirikov, J. Ford, and F. M. Izrailev, in *Stochastic Behavior of Classical and Quantum Hamiltonian Systems*, edited by C. G. and J. Ford (Springer, New York, 1979), vol. 93 of *Lecture Notes in Physics*.
- ³⁰ G. P. Berman and G. M. Zalavsky, *Physica A* **91**, 450 (1978).
- ³¹ C. Tian, A. Kamenev, and A. Larkin, *Phys. Rev. Lett.* **93**, 124101 (2004).
- ³² A. B. Rechester, M. N. Rosenbluth, and R. B. White, *Phys. Rev. A* **23**, 2664 (1981).
- ³³ J. Rammer, *Quantum Transport Theory*, vol. 99 of *Frontiers in Physics* (Perseus Books, Reading, MA, 1998).
- ³⁴ R. Blümel and U. Smilansky, *Phys. Rev. Lett.* **69**, 217 (1992).
- ³⁵ O. Bohigas, M. J. Giannoni, and C. Schmit, *Phys. Rev. Lett.* **52**, 1 (1984).
- ³⁶ A. V. Andreev, O. Agam, B. D. Simons, and B. L. Altshuler, *Phys. Rev. Lett.* **76**, 3947 (1996).
- ³⁷ O. Bohigas, in *Chaos and Quantum Physics, Proceedings of Les Houches Summer School* (1989), session LII.
- ³⁸ N. Rosenzweig and C. E. Porter, *Phys. Rev.* **120**, 1698 (1960).
- ³⁹ F. Pistolesi, *Phys. Rev. B* **69**, 245409 (2004).
- ⁴⁰ A. Altland, *Phys. Rev. Lett.* **71**, 69 (1993).
- ⁴¹ C. Tian, A. Kamenev, and A. Larkin (2004), *arXiv:cond-mat/0403482*.
- ⁴² L. S. Levitov, H. W. Lee, and G. B. Lesovik, *J. Math. Phys.* **37**, 4845 (1996).
- ⁴³ M. Kindermann and Y. V. Mazarov, *Phys. Rev. Lett.* **91**, 136802 (2003).
- ⁴⁴ Y. V. Nazarov, ed., *Noise in Mesoscopic Physics*, vol. 97 of *NATO Science Series*, Advanced Research Workshop on Quantum Noise in Mesoscopic Physics (Kluwer Academic Publisher, Delft, The Netherlands, 2003).
- ⁴⁵ M. E. Peskin and D. V. Schroeder, *An Introduction to Quantum Field Theory* (Westview Press, Reading, MA, 1995), chap. 15, pp. 491–494.
- ⁴⁶ R. Graham, M. Schlautmann, and D. L. Shepelyansky, *Phys. Rev. Lett.* **71**, 255 (1991).
- ⁴⁷ If the Cooper pair shuttling is achieved by means of time-dependent fluxes, as described in Subsection II A, $E_C(t)$ is a constant during the whole cycle.
- ⁴⁸ A Gaussian distribution function for the variables $\Delta t_b(i)$ cannot be assumed; it is inconsistent with the previous condition, $\mathcal{P}(\Delta t_b(i)) = 0$ for $\Delta t_b(i) < 0$, and, in fact, gives rise to incurable divergences due to the presence of the term $1/T$ in the expressions to be averaged.
- ⁴⁹ Periodically driven Josephson junction have been already suggested to study quantum chaos in Ref. 46.
- ⁵⁰ The generalization to the multi-terminal case is straightforward.